© 2017. Published by The Company of Biologists Ltd | Journal of Cell Science (2017) 130, 2867-2882 doi:10.1242/jcs.202408

RESEARCH ARTICLE

The E3 ubiquitin ligase NEDD4 induces endocytosis and lysosomal sorting of connexin 43 to promote loss of gap junctions

Max Z. Totland[1,2,3,4], Christian H. Bergsland[1,2,3,4], Tone A. Fykerud[1,2,4], Lars M. Knudsen[1,2,3,4], Nikoline L. Rasmussen[1,2,3,4], Peter W. Eide[1,2,4], Zeremariam Yohannes[1,2,4], Vigdis Sørensen[2,4,5], Andreas Brech[2,3,5,6], Ragnhild A. Lothe[1,2,3,4] and Edward Leithe[1,2,4,*]

ABSTRACT

Intercellular communication via gap junctions has an important role in controlling cell growth and in maintaining tissue homeostasis. Connexin 43 (Cx43; also known as GJA1) is the most abundantly expressed gap junction channel protein in humans and acts as a tumor suppressor in multiple tissue types. Cx43 is often dysregulated at the post-translational level during cancer development, resulting in loss of gap junctions. However, the molecular basis underlying the aberrant regulation of Cx43 in cancer cells has remained elusive. Here, we demonstrate that the oncogenic E3 ubiquitin ligase NEDD4 regulates the Cx43 protein level in HeLa cells, both under basal conditions and in response to protein kinase C activation. Furthermore, overexpression of NEDD4, but not a catalytically inactive form of NEDD4, was found to result in nearly complete loss of gap junctions and increased lysosomal degradation of Cx43 in both HeLa and C33A cervical carcinoma cells. Collectively, the data provide new insights into the molecular basis underlying the regulation of gap junction size and represent the first evidence that an oncogenic E3 ubiquitin ligase promotes loss of gap junctions and Cx43 degradation in human carcinoma cells.

KEY WORDS: Gap junction, Connexin, NEDD4, Ubiquitin, Degradation, Cancer

INTRODUCTION

The connexins represent a family of integral membrane proteins that are able to form intercellular channels (Sosinsky and Nicholson, 2005). These channels assemble into distinct plasma membrane domains known as gap junctions, which can consist of up to several thousand connexin protein subunits. Gap junctions enable adjacent cells to directly exchange ions and small molecules (under ~1 kDa), which include amino acids, nucleotides, and signaling mediators such as inositol trisphosphate (IP_3) and cyclic adenosine monophosphate (cAMP) (Saez et al., 2003). The connexin protein family consists of 21 members in humans, of which the most ubiquitously expressed is connexin 43 (Cx43; also known as GJA1) (Söhl and Willecke, 2003). The connexins have important roles in controlling cell growth and differentiation, and several connexins, including Cx43, have been shown to act as tumor suppressor proteins in various tissue types (Aasen et al., 2016). Cancer cells are often unable to form functional gap junctions because of aberrant post-translational regulation and intracellular trafficking of connexins (Leithe et al., 2006b; Mesnil et al., 2005). However, the molecular mechanisms underlying the aberrant regulation of connexins at the post-translational level during carcinogenesis remain poorly understood.

Connexins have a high turnover rate, exhibiting a half-life of 1.5 to 5 h in most tissue types (Laird, 2006). There is increasing evidence that modulation of the connexin endocytosis and turnover rate represents an important mechanism by which cells regulate the level of gap junctions at the plasma membrane under basal conditions (Falk et al., 2014; Johnson et al., 2013; Laing and Beyer, 1995; Laing et al., 1997; Laird, 2006; Musil et al., 2000; Qin et al., 2003; Rivedal and Leithe, 2005; VanSlyke and Musil, 2005). Moreover, many growth factors, oncogenes and tumor-promoting agents are potent inducers of connexin endocytosis and degradation (Bager et al., 1994; Guan and Ruch, 1996; Krutovskikh et al., 1995; Mograbi et al., 2003; Oh et al., 1991). Endocytosis of gap junctions involves the formation of a double-membrane vacuole called an annular gap junction or connexosome. Increasing evidence suggests that Cx43 can follow different pathways en route to lysosomes (Falk et al., 2014; Leithe et al., 2012). One pathway involves the direct fusion of annular gap junctions and lysosomes (Murray et al., 1981; Naus et al., 1993; Qin et al., 2003; Vaughan and Lasater, 1990). In another pathway, annular gap junctions are engulfed by autophagosomes, which subsequently fuse with lysosomes (Carette et al., 2015; Fong et al., 2012; Hesketh et al., 2010; Lichtenstein et al., 2011). We have previously proposed that a third pathway for degradation of connexins also exists, in which the annular gap junction undergoes a morphological transition to form a Cx43-enriched multivesicular endosome consisting of a single limiting membrane (Fykerud et al., 2012; Leithe et al., 2006a, 2009). This pathway involves the fusion between annular gap junctions and early endosomes, and the subsequent sorting of Cx43 to lysosomes via the endolysosomal pathway.

Emerging evidence indicates that Cx43 is post-translationally regulated by ubiquitylation (Basheer et al., 2015; Bejarano et al., 2012; Catarino et al., 2011; Chen et al., 2012; Girao et al., 2009; Laing and Beyer, 1995; Leithe and Rivedal, 2004a,b, 2009; Leithe, 2016; Smyth et al., 2014). Moreover, there appears to be a close relationship between Cx43 phosphorylation and ubiquitylation. Exposure of cells to the tumor promoter 12-O-tetradecanoylphorbol 13-acetate (TPA) results in increased phosphorylation of Cx43, which is associated with inhibition of gap junctional intercellular communication (Berthoud et al., 1993; Enomoto et al., 1984;

[1]Department of Molecular Oncology, Institute for Cancer Research, Oslo University Hospital, 0424 Oslo, Norway. [2]Centre for Cancer Biomedicine, Faculty of Medicine, University of Oslo, 0316 Oslo, Norway. [3]Institute for Biosciences, University of Oslo, 0316 Oslo, Norway. [4]K.G. Jebsen Colorectal Cancer Research Centre, Oslo University Hospital, 0424 Oslo, Norway. [5]Department of Core Facilities, Institute for Cancer Research, Oslo University Hospital, 0424 Oslo, Norway. [6]Department of Molecular Cell Biology, Institute for Cancer Research, Oslo University Hospital, 0424 Oslo, Norway.

*Author for correspondence (eleithe@rr-research.no)

E.L., 0000-0003-0831-2642

Received 13 February 2017; Accepted 12 July 2017

Journal of Cell Science

Journal of Cell Science (2017) 130, 2867-2882 doi:10.1242/jcs.202408

Lampe, 1994; Leithe et al., 2003; Murray and Fitzgerald, 1979; Rivedal et al., 1994). The TPA-induced phosphorylation of Cx43 is mediated via protein kinase C (PKC), and may also involve extracellular signal-regulated protein kinases 1 and 2 (ERK1/2) (Rivedal and Opsahl, 2001; Ruch et al., 2001; Sirnes et al., 2009). TPA has also been shown to promote endocytosis and degradation of Cx43 (Asamoto et al., 1991; Leithe and Rivedal, 2004b; Matesic et al., 1994). The TPA-induced endocytosis and degradation of Cx43 is associated with increased Cx43 ubiquitylation (Leithe and Rivedal, 2004b). Under these conditions, ubiquitylation may act as a signal for sorting of Cx43 along the endolysosomal pathway (Leithe et al., 2009). Cx43 ubiquitylation has also been shown to increase during epidermal growth factor (EGF)-induced endocytosis and degradation of gap junctions (Chen et al., 2012; Leithe and Rivedal, 2004a). However, the molecular basis underlying the regulation of Cx43 ubiquitylation and the functional consequences of this modification on gap junction size are still poorly understood. It has also been suggested that Cx43 ubiquitylation may not be involved in regulating gap junction stability (Dunn et al., 2012).

The 'homologous to E6-AP C-terminus' (HECT) family of E3 ubiquitin ligases comprises 28 members in humans (Bernassola et al., 2008). This protein family is characterized by an ∼350-residue region at their C-termini, termed the HECT domain (Huibregtse et al., 1995). The HECT domain contains a strictly conserved cysteine residue, which acts as a site for thiol ester formation with ubiquitin transferred from an E2 conjugating enzyme. Among the best-studied members of the HECT E3 ubiquitin ligase family is neural precursor cell-expressed developmentally downregulated gene 4 (NEDD4) (Boase and Kumar, 2015). NEDD4 has been shown to be overexpressed in various cancer types and is considered a proto-oncogene (Zou et al., 2015). The ability of NEDD4 to act as an oncogene has been attributed to its ability to mediate the ubiquitylation and degradation of the tumor suppressor protein phosphatase and tensin homolog (PTEN) (Amodio et al., 2010; Wang et al., 2007). However, increasing evidence suggests that NEDD4 may also promote cancer cell growth independently of PTEN (Eide et al., 2013; Zou et al., 2015). NEDD4 is a potential target protein in cancer therapy, and obtaining a clearer understanding of the role of NEDD4 in cancer pathogenesis may therefore have future clinical implications (Ye et al., 2014).

NEDD4 has been shown to interact with Cx43 (Girao et al., 2009; Leykauf et al., 2006; Spagnol et al., 2016). Binding between NEDD4 and Cx43 involves a proline-rich region in the C-terminal tail of Cx43 that corresponds to the consensus of a PY (xPPxY, where P is proline, x is any amino acid and Y is tyrosine) motif. Leykauf et al. found that depletion of NEDD4 by siRNA results in increased Cx43 gap junction size, suggesting that NEDD4 may be involved in modulating the endocytosis of Cx43 (Leykauf et al., 2006). Subsequent studies by Girão et al. suggested that NEDD4-mediated ubiquitylation of Cx43 acts as a signal for recruitment of the ubiquitin-binding protein epidermal growth factor receptor substrate 15 (Eps15), which mediates gap junction endocytosis (Girao et al., 2009). However, in neither of these two studies did depletion of NEDD4 affect the cellular level of Cx43, suggesting that NEDD4 may not be involved in regulating Cx43 degradation under basal conditions. In a more recent study, Bejarano et al. showed that NEDD4 mediates the autophagy-mediated degradation of Cx43 in response to serum starvation (Bejarano et al., 2012). However, the role of NEDD4 in regulating Cx43 protein levels under basal conditions has remained elusive.

The objective of the present study was to obtain a better understanding of the role of NEDD4 in the regulation of Cx43 degradation and gap junction size. Moreover, since NEDD4 is a proto-oncogene and is frequently overexpressed in human carcinomas, we aimed to investigate how overexpression of NEDD4 in carcinoma cells affects Cx43 protein and gap junction size. As cellular model systems, the human cervical carcinoma cell lines HeLa and C33A were used, since cervical cancer is known to be associated with aberrant post-translational regulation of Cx43 and loss of functional gap junctions (Aasen et al., 2003, 2005; King et al., 2000a,b). The data demonstrate that NEDD4 controls the Cx43 protein level in HeLa cells both under basal conditions and in response to PKC activation. Evidence is further provided that overexpression of NEDD4 results in loss of gap junctions in both HeLa and C33A cells, in a process that requires a functional HECT domain.

RESULTS

The constitutive and PKC-induced degradation of Cx43 in HeLa cells involves the endolysosomal system

Degradation of Cx43 in HeLa cells has previously been shown to involve the autophagosomal pathway (Carette et al., 2015; Fong et al., 2012). However, to our knowledge, the potential role of the endolysosomal pathway in the degradation of Cx43 in HeLa cells under basal conditions or in response to PKC activation has not been examined. As a first approach to investigate the role of the endolysosomal pathway in the degradation of Cx43 in HeLa cells, we analyzed the subcellular localization of Cx43 in HeLa cells stably transfected with Cx43 (HeLa-Cx43 cells) by super-resolution microscopy. As determined by structured illumination microscopy (SIM), untreated HeLa-Cx43 cells displayed large Cx43 gap junctions at intercellular appositions and some Cx43 staining in intracellular vesicular compartments (Fig. 1A), in accordance with previous studies (Elfgang et al., 1995). Treatment of cells with TPA resulted in increased endocytosis of gap junctions (Fig. 1B). The Cx43-positive intracellular structures observed in response to TPA treatment were frequently positive for early endosome antigen 1 (EEA1), a marker for early endosomes, or lysosome-associated membrane glycoprotein 1 (LAMP1), a marker for late endosomes and lysosomes (Fig. 1C,D). Cx43 often appeared to localize in the lumen of the EEA1-positive or LAMP1-positive vesicular compartments (Fig. 1C,D). Notably, Cx43 was also found to localize in EEA1- and LAMP1-positive vesicular compartments in untreated HeLa-Cx43 cells (Fig. S1A,B). Sometimes, the Cx43-positive intracellular vesicles in TPA-treated cells appeared to have a somewhat irregular border rather than the appearance of typical annular gap junctions. To further characterize these structures, we performed three-dimensional reconstruction of Cx43-positive structures. This analysis revealed that the Cx43-positive vesicular structures with irregular shapes often appeared to be undergoing fusion with EEA1-positive structures (Fig. S2). Thus, one potential explanation for the irregular border of some of the Cx43-positive structures may be that they are in the process of fusing with early endosomes.

In addition to the localization of Cx43 in gap junctions and in endocytic vesicles, there also appeared to be an intracellular pool of Cx43-positive vesicles in the size range of secretory vesicles, as determined by super-resolution microscopy (Fig. 1A,B) and confocal fluorescence microscopy (Fig. S3A). Such vesicles were observed under both basal conditions as well as in cells treated with TPA. To differentiate between a possible effect of TPA on Cx43 localized in the secretory pathway from the effect on Cx43 localized in gap junctions, the Cx43 pool residing in the secretory pathway was depleted by treating the cells with the protein synthesis inhibitor

Journal of Cell Science (2017) 130, 2867-2882 doi:10.1242/jcs.202408

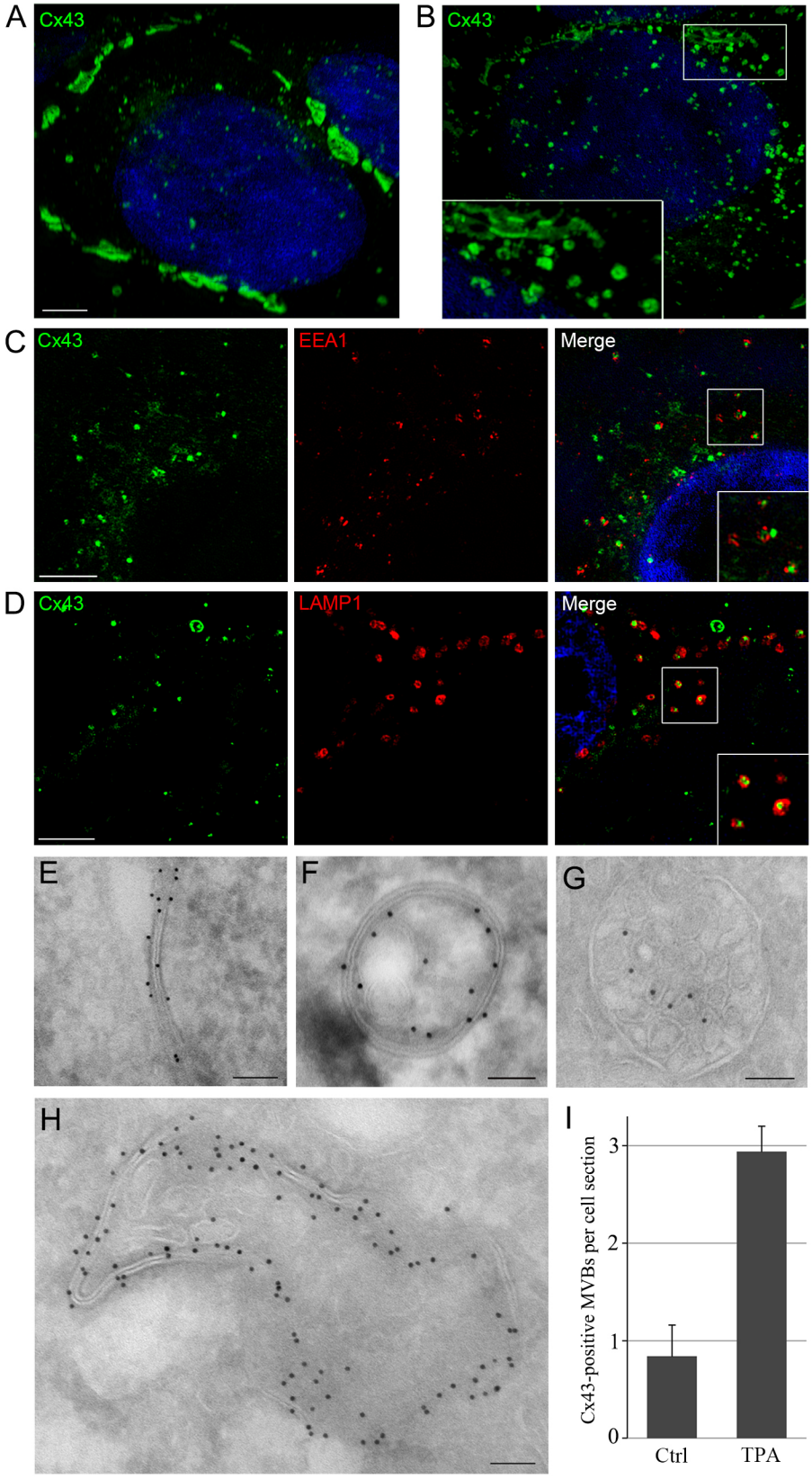

Fig. 1. Super-resolution and immunoelectron microscopy analysis of the subcellular localization of Cx43 in HeLa-Cx43 cells. (A,B) HeLa-Cx43 cells were left untreated (A) or treated with TPA (100 ng/ml) for 90 min (B). The cells were fixed and stained with anti-Cx43 (green) antibodies followed by Alexa Fluor 488-conjugated secondary antibodies. Nuclei were stained with Hoechst 33342 (blue). Cells were imaged by SIM, and images were subjected to three-dimensional reconstruction using IMARIS software. Scale bar: 3 µm (applies to both images). (C) HeLa-Cx43 cells were treated with TPA (100 ng/ml) for 90 min. The cells were fixed and stained with anti-Cx43 (green) and anti-EEA1 (red) antibodies followed by Alexa Fluor 488- and Alexa Fluor 555-conjugated secondary antibodies. Cells were imaged by SIM and shown is a single section from a SIM *z*-stack. Scale bar: 3 µm. (D) HeLa-Cx43 cells were treated with TPA (100 ng/ml) for 90 min. The cells were fixed, stained with anti-Cx43 (green) and anti-LAMP1 (red) antibodies followed by Alexa Fluor 488- and Alexa Fluor 555-conjugated secondary antibodies. Cells were imaged by SIM and shown is a single section from a SIM *z*-stack. Scale bar: 4 µm. (E–H) Cells were treated with TPA (100 ng/ml) for 60 min (E–G) or left untreated (H) and fixed for immunoelectron microscopy. Ultrathin cryosections were labeled for Cx43 by using anti-Cx43 antibodies, followed by incubation with 10 nm Protein-A–gold particles. Scale bars: 100 nm. (I) Quantification of the number of Cx43-positive multivesicular bodies (MVBs) per cell section in untreated (ctrl) and TPA-treated HeLa-Cx43 cells. Values shown are the means±s.e.m. of two independent experiments. In each experiment, 50 cell sections of untreated and TPA-treated HeLa-Cx43 cells were analyzed.

cycloheximide for 2 h prior to TPA treatment. As expected, in response to cycloheximide treatment for 2 h, the Cx43-positive vesicles that were in the size range of secretory vesicles disappeared (Fig. S3A). Moreover, whereas control cells displayed a faint Cx43 staining in the perinuclear area, presumably representing newly synthesized Cx43 localized in the Golgi and the trans-Golgi network, cycloheximide-treated cells did not display such diffuse perinuclear staining of Cx43 (Fig. S3A). Notably, TPA, but not

Journal of Cell Science (2017) 130, 2867-2882 doi:10.1242/jcs.202408

solvent (DMSO) alone, was found to induce an increase in Cx43-positive vesicles in cells preincubated with cycloheximide for 2 h, similar to what was observed in cells not subjected to the cycloheximide preincubation (Fig. S3A). Moreover, the TPA-induced Cx43-positive vesicles were, under these conditions, often found to partly colocalize with EEA1 (Fig. S3B). Collectively, these observations support the notion that the increase in intracellular Cx43-positive vesicular structures in response to TPA treatment is due to increased endocytosis of gap junctions rather than a block in the transport of Cx43-positive vesicles along the secretory pathway.

Some of the Cx43-positive structures observed in response to TPA treatment could represent parts of the plasma membrane that are projecting into the cytoplasm rather than completely detached annular gap junctions. To differentiate between these possibilities, cells were first treated with TPA for 90 min and then the plasma membrane was stained with wheat germ agglutinin (WGA) (Fig. S4A). The majority of the intracellular Cx43-positive vesicular structures observed in response to TPA treatment did not colocalize with WGA, suggesting that these structures were completely detached from the plasma membrane (Fig. S4A). Notably, when the plasma membrane was stained with WGA prior to TPA treatment for 90 min, Cx43 was found to partly colocalize with WGA in intracellular vesicular compartments, in line with the above conclusion that the increase in Cx43-positive intracellular vesicular compartments observed in response to TPA treatment is due to increased Cx43 endocytosis (Fig. S4B).

We next analyzed the subcellular localization of Cx43 in HeLa-Cx43 cells by immunoelectron microscopy. As expected, Cx43 immunogold staining was observed in gap junctions in untreated HeLa-Cx43 cells (Fig. S5A). Some gap junctions were also observed following treatment of HeLa-Cx43 cells with TPA for 60 min (Fig. 1E). However, under these conditions, most Cx43 staining was found in intracellular vesicular compartments. Many of these compartments appeared to represent annular gap junctions, which have previously been shown to correspond to endocytosed gap junctions (Fig. 1F; Fig. S5B). In these structures, the typical Cx43 staining pattern was along the limiting double membrane. Cx43 staining was also observed in multivesicular endosomes, in which Cx43 typically displayed diffuse labeling across the section of the endosome (Fig. 1G; Fig. S5C). A similar Cx43 staining pattern in annular gap junctions and multivesicular endosomes was also observed in untreated HeLa-Cx43 cells (Fig. 1H; Fig. S5A,D). Annular gap junctions were sometimes found to contain small single-membrane intraluminal vesicles that were positive for Cx43 that resembled the intraluminal vesicles of multivesicular endosomes (Fig. 1H). The presence of such small vesicles inside the annular gap junction appeared to be associated with disruption of its double-membrane structure. We have previously reported on similar Cx43-positive intraluminal vesicles inside gap junctions in IAR20 cells (Leithe et al., 2006a). We have proposed that such structures may represent annular gap junctions undergoing a maturation process from a double-membrane vesicle to a Cx43-enriched multivesicular endosome containing a single limiting membrane. To our knowledge, this is the first evidence that similar processing of annular gap junctions also occurs in HeLa-Cx43 cells.

Quantification of the Cx43 immunogold labeling indicated that there was an ∼3-fold increase in the number of Cx43-positive multivesicular bodies in HeLa-Cx43 cells following TPA treatment compared with control cells (Fig. 1I).

Taken together, these data indicate that TPA induces increased endocytosis of Cx43 gap junctions in HeLa-Cx43 cells. The data further suggest that, in addition to involving the autophagosomal pathway as reported previously, degradation of Cx43 in HeLa-Cx43 cells involves the endolysosomal pathway, both under basal conditions and in response to TPA treatment.

TPA induces PKC-mediated Cx43 ubiquitylation and degradation in HeLa cells

To analyze the effect of TPA on Cx43 degradation in HeLa-Cx43 cells, we treated the cells with TPA in combination with cycloheximide, or with cycloheximide alone, for various times up to 3 h. The Cx43 protein levels were then determined by western blotting. In accordance with previous studies, Cx43 formed several distinct bands when analyzed by SDS-PAGE and western blotting (Fig. 2A) (Solan and Lampe, 2009). The faster-migrating band localized at ∼38 kDa has previously been shown to include non-phosphorylated Cx43 and is commonly termed P0. The two slower-migrating forms at 41 and 43 kDa, termed P1 and P2, respectively, represent different phosphorylation states of Cx43 (Solan and Lampe, 2009). A weak Cx43 band was also detected at 50 kDa. TPA treatment resulted in an increase in the relative intensity of the P1 and P2 bands compared with the P0 band, in accordance with the notion that the phosphorylation status of Cx43 is affected by TPA exposure. Furthermore, TPA treatment significantly increased Cx43 degradation, as compared with exposure of cells to cycloheximide alone (Fig. 2A,B). As control, treatment of cells with diluent (DMSO) did not affect the subcellular localization of Cx43 (Fig. S6A) or the Cx43 protein level (Fig. S6B,C). As determined by confocal fluorescence microscopy, TPA-induced endocytosis of Cx43 was strongly counteracted by the PKC inhibitor GF109203X, suggesting that the effect is mediated by PKC (Fig. 2C). The PKC inhibitor was also found to counteract TPA-induced degradation of Cx43, as determined by quantitative western blotting (Fig. 2D) and confocal fluorescence microscopy (Fig. 2E). Notably, there were considerably fewer Cx43-positive structures within the cytoplasm following co-treatment of cells with TPA and cycloheximide for 3 h (Fig. 2E) as compared to when cells were treated with TPA for 1 h (Fig. 2C). This observation is in accordance with the notion that after 1 h of TPA treatment, a large pool of Cx43 has become endocytosed but not yet degraded, whereas following treatment with TPA for 3 h, a large fraction of the cellular pool of Cx43 has been degraded, resulting in reduced numbers of Cx43-positive vesicular structures.

To analyze the effect of TPA on the Cx43 ubiquitylation status and the role of PKC in this process, HeLa-Cx43 cells were left untreated or treated with TPA for 30 min in the presence or absence of GF109203X. Cx43 was then subjected to immunoprecipitation, and Cx43 ubiquitylation was detected by western blotting using anti-ubiquitin antibodies (Fig. 2F). The ubiquitylated form of Cx43 in HeLa-Cx43 cells appeared as a smear with the highest intensity at around 50 kDa (Fig. 2F). Given that the molecular mass of ubiquitin is ∼8.5 kDa, the smear around 50 kDa presumably represents the monoubiquitylated form of Cx43. TPA treatment resulted in increased Cx43 ubiquitylation in HeLa-Cx43 cells (Fig. 2F). As determined by quantification of the intensity of the ubiquitylated Cx43 on western blots, the Cx43 ubiquitylation level was increased by ∼60% in cells exposed to TPA for 30 min compared with untreated cells (Fig. 2G). The TPA-induced increase in Cx43 ubiquitylation was counteracted by GF109203X, suggesting that the process is mediated by PKC. Taken together, these data indicate that Cx43 is ubiquitylated under basal conditions in HeLa-Cx43 cells and that exposure of HeLa-Cx43 cells to TPA results in increased ubiquitylation, endocytosis and degradation of Cx43 in a process mediated by PKC.

Journal of Cell Science (2017) 130, 2867-2882 doi:10.1242/jcs.202408

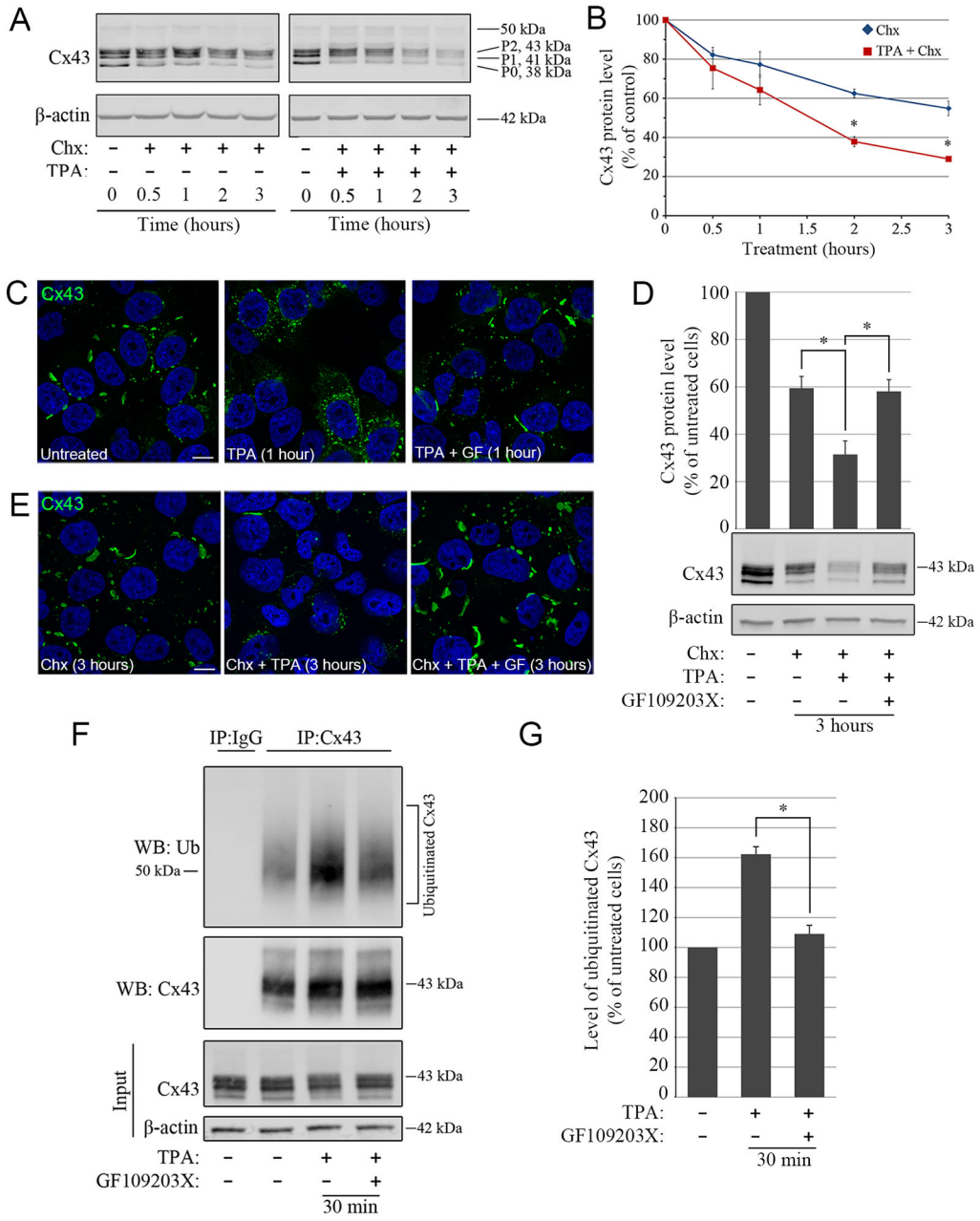

Fig. 2. Effect of TPA on Cx43 ubiquitylation, endocytosis and degradation in HeLa-Cx43 cells. (A) HeLa-Cx43 cells were treated with cycloheximide (Chx, 10 µM) alone or in combination with TPA (100 ng/ml) for the given periods. Cell lysates were then prepared and equal amounts of total cell protein were subjected to SDS-PAGE. Cx43 (P0, P1 and P2 forms) and β-actin were detected by western blotting, using anti-Cx43 and anti-β-actin antibodies, respectively. Molecular mass in kDa is indicated. (B) The intensities of the Cx43 bands shown in A were quantified and normalized to the level of β-actin. Values shown are the mean±s.e.m. of three independent experiments. **P*<0.05. (C) HeLa-Cx43 cells were left untreated or treated with TPA (100 ng/ml) alone or in combination with GF109203X (GF,10 µM) for 60 min. Methanol (solvent for GF109203X) was added to cells not treated with GF109203X. Cx43 was visualized by confocal fluorescence microscopy. Scale bar: 10 µm (applies to all images). (D) HeLa-Cx43 cells were left untreated or treated with cycloheximide (Chx, 10 µM) alone or in combination with TPA (100 ng/ml) and GF109203X (10 µM), as indicated, for 3 h. Methanol (solvent) was added to cells not treated with GF109203X. Cell lysates were then prepared and equal amounts of total cell protein were subjected to SDS-PAGE. Cx43 and β-actin were detected by western blotting, using anti-Cx43 and anti-β-actin antibodies, respectively. The intensities of the Cx43 bands were quantified and normalized to the level of β-actin. Values shown are the mean±s.e.m. of five independent experiments. **P*<0.01. Molecular mass in kDa is indicated. (E) HeLa-Cx43 cells were left untreated or treated with cycloheximide (Chx, 10 µM) alone or in combination with TPA (100 ng/ml) and GF109203X (GF, 10 µM) as indicated for 3 h. Methanol (solvent) was added to cells not treated with GF109203X. The cells were fixed, stained with anti-Cx43 antibodies, and visualized by confocal fluorescence microscopy. Scale bar: 10 µm (applies to all images). (F) HeLa-Cx43 cells were treated with TPA (100 ng/ml) in combination with GF109203X (10 µM) or methanol (solvent), as indicated, for 30 min. Cell lysates were then subjected to immunoprecipitation (IP) by using anti-Cx43 antibodies or with rabbit IgG as control, and equal amounts of immunoprecipitates were subjected to SDS-PAGE. Ubiquitylated Cx43 was detected by western blotting (WB) using anti-ubiquitin antibodies (upper panel). The blot was stripped and reprobed with anti-Cx43 antibodies (lower panel). Also shown is the relative expression of Cx43 and β-actin in cell lysates prior to immunoprecipitation (Input). Molecular mass in kDa is indicated. (G) Quantification of ubiquitylated Cx43 based on the data obtained in F. For each lane, the level of ubiquitin immunoreactivity was normalized to the level of Cx43 immunoreactivity. Values shown are the means±s.e.m. of three independent experiments. **P*<0.01.

Journal of Cell Science (2017) 130, 2867-2882 doi:10.1242/jcs.202408

NEDD4 controls the Cx43 protein level and gap junction size in HeLa-Cx43 cells under basal conditions

NEDD4 has previously been shown to mediate the degradation of Cx43 by autophagy in response to serum starvation (Bejarano et al., 2012). However, the role of NEDD4 in the regulation of Cx43 protein levels under normal cell growth conditions has remained unclear. Cervical cancer pathogenesis is associated with the loss of Cx43 expression and gap junctions (Aasen et al., 2003, 2005; King et al., 2000a,b). HeLa-Cx43 cells were therefore considered a suitable model system for studying the role of NEDD4 in the regulation of Cx43 and gap junction size in human carcinoma cells. As a first approach to investigate its role in the regulation of Cx43 in HeLa-Cx43 cells, we examined whether NEDD4 forms a complex with Cx43 in these cells. In these experiments, plasmids encoding HA-tagged NEDD4 (HA–NEDD4) were transfected into HeLa-Cx43 cells, and Cx43 was then subjected to immunoprecipitation. As determined by western blotting, Cx43 was found to co-immunoprecipitate with HA–NEDD4, suggesting that HA–NEDD4 and Cx43 form a complex in HeLa-Cx43 cells (Fig. 3A).

To investigate the role of NEDD4 in the regulation of Cx43 under basal conditions, HeLa-Cx43 cells were depleted of NEDD4 by conducting a 96-h transfection with an siRNA sequence targeting NEDD4. The depletion of NEDD4 was associated with a strong increase in Cx43 protein levels, as determined by western blotting (Fig. 3B). Quantification of the Cx43 bands on western blots suggested that the level of Cx43 in cells depleted of NEDD4 was ~60% higher compared with that in control siRNA-transfected cells (Fig. 3B). Similar effects of NEDD4 depletion on Cx43 protein levels were observed when four independent siRNA sequences targeting NEDD4 were used (Fig. S7). In accordance with the western blot analysis, the depletion of NEDD4 was associated with enlarged gap junctions at the plasma membrane, as determined by confocal fluorescence microscopy (Fig. 3C). Taken together, these data indicate that NEDD4 is involved in regulating Cx43 protein levels and gap junction size under basal conditions in HeLa-Cx43 cells.

NEDD4 mediates PKC-induced endocytosis and degradation of Cx43 in HeLa cells

Next, we asked whether NEDD4 is involved in mediating PKC-induced degradation of Cx43. To this end, HeLa-Cx43 cells were transfected with siRNA targeting NEDD4 or with control siRNA, and the cells were co-treated with TPA and cycloheximide for various times up to 3 h. Cx43 protein levels at these time points were then analyzed by western blotting (Fig. 4A). A quantitative analysis of the Cx43 signal indicated that cells depleted of NEDD4 displayed reduced degradation of Cx43 in response to TPA treatment compared with that in control-siRNA-transfected cells (Fig. 4B). The notion that NEDD4 mediates the TPA-induced degradation of Cx43 was also supported by confocal fluorescence microscopy

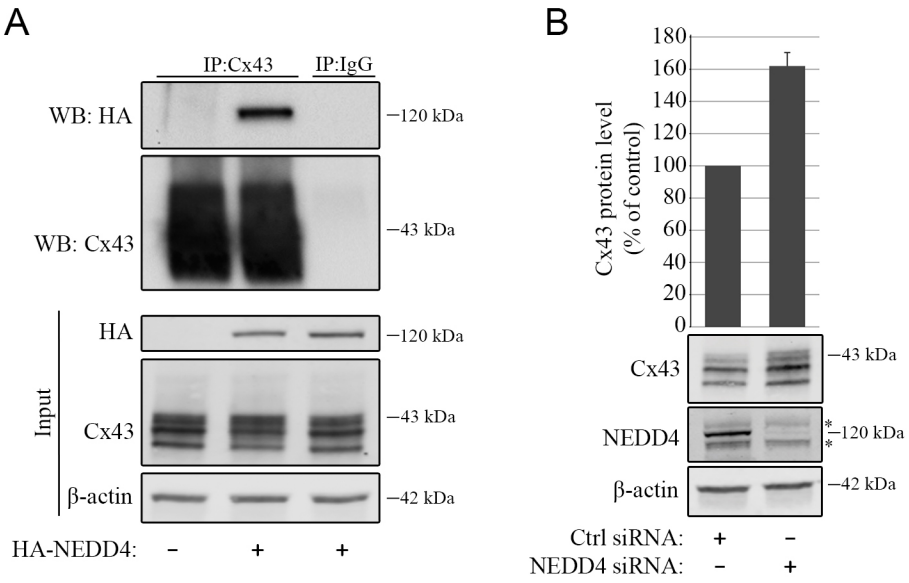

Fig. 3. Role of NEDD4 in regulating the Cx43 protein level and gap junction size in HeLa-Cx43 cells. (A) HeLa-Cx43 cells were transfected with HA–NEDD4 (wild type) or empty vector, as indicated. Cell lysates were subjected to immunoprecipitation (IP) with anti-Cx43 antibodies or with rabbit IgG as control. Equal amounts of immunoprecipitates were subjected to SDS-PAGE. Co-immunoprecipitated HA-NEDD4 was detected by western blotting (WB) using anti-HA antibodies (upper panel) and immunoprecipitated Cx43 was detected by using anti-Cx43 antibodies (lower panel). Molecular mass in kDa is indicated. (B) HeLa-Cx43 cells were transfected with control (Ctrl) siRNA or with an siRNA sequence against NEDD4. Cell lysates were prepared 96 h after transfection, and equal amounts of total cell protein lysates were subjected to SDS-PAGE. NEDD4, Cx43 and β-actin were detected by western blotting. The intensities of the Cx43 bands on western blots were quantified and normalized to the β-actin level. Asterisks indicate unspecific bands. Values shown are the mean±s.e.m. of three independent experiments. Molecular mass in kDa is indicated. (C) HeLa-Cx43 cells were transfected with control siRNA or with an siRNA sequence against NEDD4 for 96 h. Cx43 was visualized by confocal fluorescence microscopy. Scale bar: 10 µm (applies to both images).

Journal of Cell Science (2017) 130, 2867-2882 doi:10.1242/jcs.202408

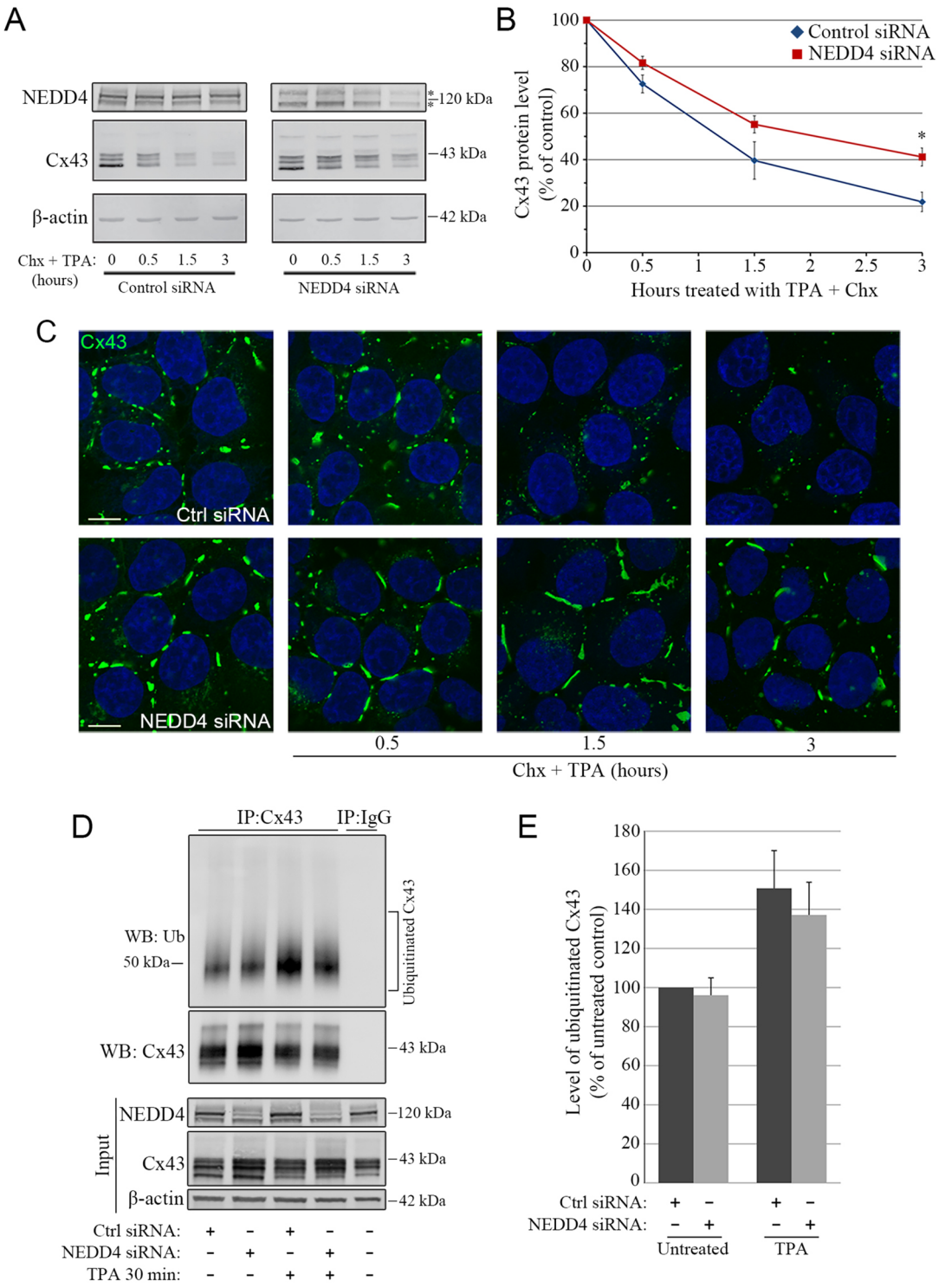

Fig. 4. Role of NEDD4 in TPA-induced endocytosis and degradation of Cx43. HeLa-Cx43 cells were transfected with control siRNA or with an siRNA sequence against NEDD4. (A) HeLa-Cx43 cells were treated with cycloheximide (Chx, 10 µM) in combination with TPA (100 ng/ml) for the given periods. Cell lysates were then prepared and equal amounts of total cell protein were subjected to SDS-PAGE. Cx43 and β-actin were detected by western blotting. Asterisks indicate unspecific bands. Molecular mass in kDa is indicated. (B) The intensities of the Cx43 bands shown in A were quantified and normalized to the level of β-actin. Values shown are the means±s.e.m. of three independent experiments. *P<0.05. (C) HeLa-Cx43 cells were treated with cycloheximide (Chx, 10 µM) in combination with TPA (100 ng/ml) for the given periods. Cx43 was visualized by confocal fluorescence microscopy. Scale bars: 10 µm. (D) HeLa-Cx43 cells were transfected with control siRNA or with siRNA against NEDD4. After 96 h of transfection, cells were left untreated or treated with TPA (100 ng/ml) for 30 min. Cells were then subjected to immunoprecipitation (IP) with anti-Cx43 antibodies or with rabbit IgG as control. Equal amounts of immunoprecipitates were subjected to SDS-PAGE, and ubiquitylated Cx43 was detected by western blotting (WB; upper panel). The blot was stripped and reprobed with anti-Cx43 antibodies (lower panel). Also shown is the relative expression of Cx43 and β-actin in cell lysates prior to immunoprecipitation (Input). Molecular mass in kDa is indicated. (E) Quantification of ubiquitylated Cx43 based on the data obtained in D. For each lane, the level of ubiquitin immunoreactivity was normalized to the level of Cx43 immunoreactivity. Values shown are the means±s.e.m. of three independent experiments.

Journal of Cell Science (2017) 130, 2867-2882 doi:10.1242/jcs.202408

studies (Fig. 4C). As expected, control-siRNA-transfected cells co-treated with TPA and cycloheximide for 3 h had reduced overall Cx43 staining and smaller gap junctions at the plasma membrane compared with untreated cells (Fig. 4C). In contrast, cells depleted of NEDD4 displayed more intense overall Cx43 staining and larger gap junctions between adjacent cells after exposure to TPA and cycloheximide for 3 h. On the basis of these observations, we conclude that NEDD4 is involved in mediating PKC-induced endocytosis and degradation of Cx43.

To analyze the effect of NEDD4 depletion on the Cx43 ubiquitylation status, control-siRNA-transfected HeLa-Cx43 cells or cells depleted of NEDD4 were left untreated or treated with TPA for 30 min, and Cx43 was subjected to immunoprecipitation. The Cx43 ubiquitylation status was then determined by western blotting (Fig. 4D,E). The depletion of NEDD4 did not have a statistically significant effect on the overall Cx43 ubiquitylation status, neither in untreated cells nor in response to TPA treatment (Fig. 4D,E). The lack of an apparent effect on the overall Cx43 ubiquitylation in response to depletion of NEDD4 may be due to NEDD4 catalyzing the ubiquitylation of one or only a few lysine residues in Cx43 (see Discussion).

NEDD4 promotes loss of gap junctions in HeLa-Cx43 cells

NEDD4 has previously been shown to act as a proto-oncogene and is frequently overexpressed in various cancer types (Zou et al., 2015). We therefore aimed to examine the effect of overexpression of NEDD4 on Cx43 protein and gap junction size in HeLa-Cx43 cells. Importantly, as determined by confocal fluorescence microscopy, transfection of wild-type HA–NEDD4 (HA–NEDD4-WT) in HeLa-Cx43 cells was found to result in a nearly complete loss of gap junctions between adjacent cells (Fig. 5A,B). In contrast, transfecting the cells with HA–NEDD4-C867A, containing an inactivating mutation in the catalytic cysteine residue of the HECT domain, did not appear to have any effect on the gap junctions (Fig. 5C,D).

To examine the effect of ectopic overexpression of NEDD4 on Cx43 protein levels, we transfected HeLa-CCL2 cells, which express only miniscule levels of endogenous Cx43, with Cx43 alone or with Cx43 in combination with HA–NEDD4-WT or HA–NEDD4-C867A. As determined by western blotting, co-transfection of HA–NEDD4-WT resulted in reduced Cx43 protein levels compared with cells transfected with Cx43 alone (Fig. 6A). Quantification of western blots revealed that cells co-transfected with Cx43 and HA–NEDD4-WT exhibited a Cx43 protein level that

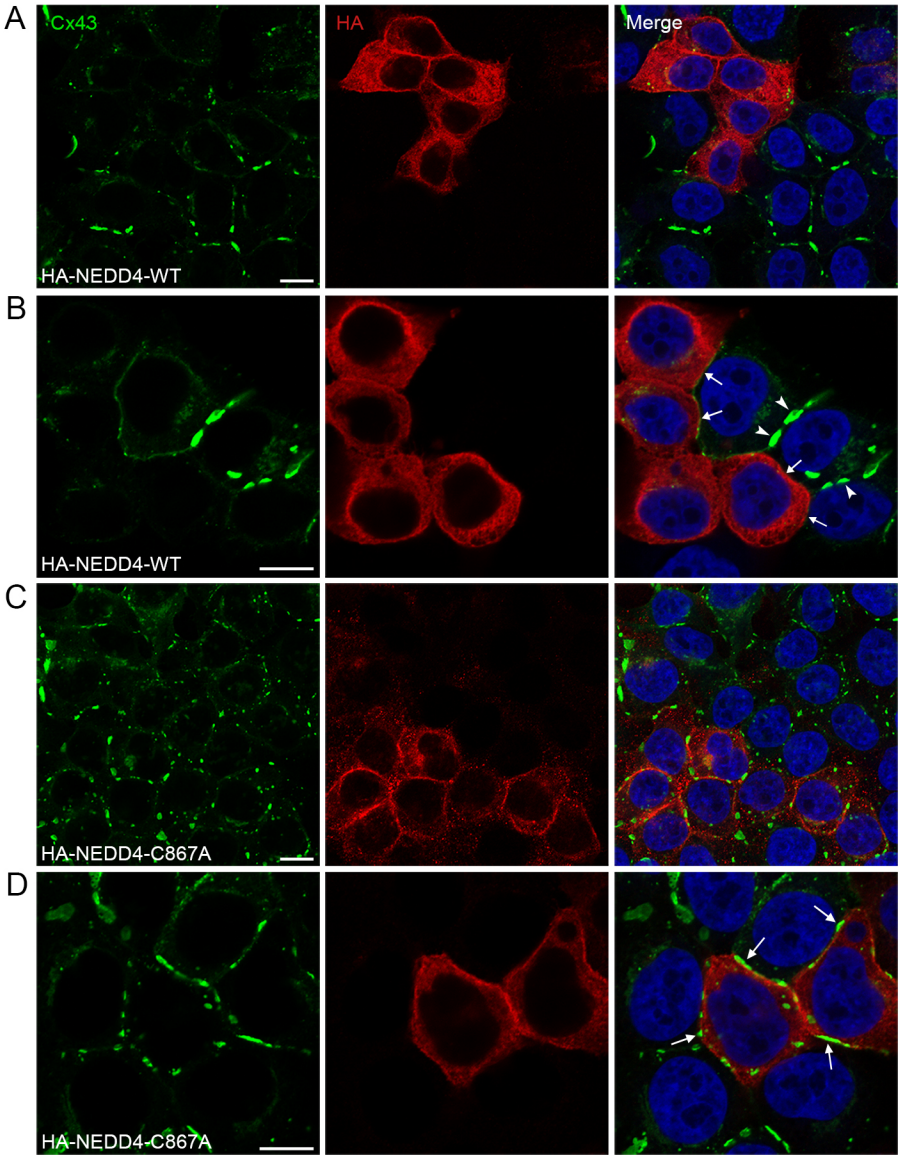

Fig. 5. Effect of ectopic overexpression of NEDD4 on the Cx43 subcellular localization in HeLa-Cx43 cells. HeLa-Cx43 cells were transfected with HA–NEDD4-WT (A,B) or HA–NEDD4-C867A for 48 h (C,D). Cx43 (green) and HA (red) were visualized by confocal fluorescence microscopy. Scale bars: 10 µm. Arrowheads in B indicate the presence of gap junctions between HeLa-Cx43 cells that are not transfected with HA–NEDD4-WT. Arrows in B indicate plasma membrane regions between non-transfected cells and cells transfected with HA–NEDD4-WT in which gap junctions are not formed. Arrows in D indicate the presence of gap junctions between cells that are not transfected and cells that have been transfected with HA–NEDD4-C867A.

Journal of Cell Science (2017) 130, 2867-2882 doi:10.1242/jcs.202408

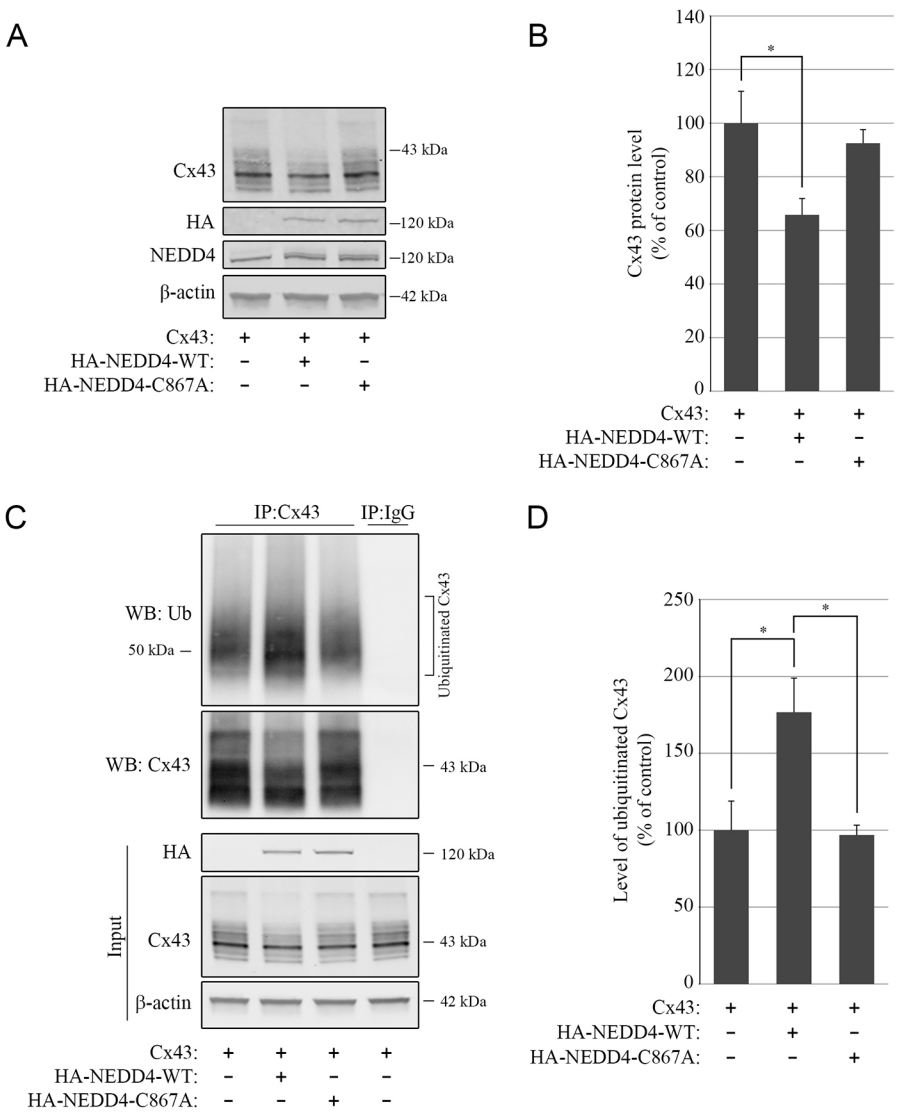

Fig. 6. Effect of ectopic overexpression of NEDD4 on Cx43 protein level and ubiquitylation status in HeLa cells. (A) HeLa-CCL2 cells were co-transfected with Cx43 and empty vector or with Cx43 and HA–NEDD4-WT or HA–NEDD4-C867A for 48 h, as indicated. Cell lysates were then prepared and equal amounts of total cell protein were subjected to SDS-PAGE. Cx43 and β-actin were detected by western blotting. Molecular mass in kDa is indicated. (B) The intensities of the Cx43 bands on western blots shown in A were quantified and normalized to the level of β-actin. Values shown are the means±s.e.m. of five independent experiments. *P<0.05. (C) HeLa-CCL2 cells were co-transfected with Cx43 and empty vector, Cx43 and HA–NEDD4-WT, or Cx43 and HA–NEDD4-C867A for 48 h, as indicated. Cell lysates were then subjected to immunoprecipitation (IP) using anti-Cx43 antibodies. Ubiquitylated Cx43 was detected by western blotting (WB) using anti-ubiquitin antibodies. The blots were stripped and reprobed using anti-Cx43 antibodies. Also shown is the relative expression of Cx43 and β-actin in cell lysates prior to immunoprecipitation (Input). Molecular mass in kDa is indicated. (D) Quantification of ubiquitylated Cx43 based on western blots shown in C. For each lane, the level of ubiquitin immunoreactivity was normalized to the level of Cx43 immunoreactivity. Values shown are the means±s.e.m. of four independent experiments. *P<0.05.

was ∼65% of that in cells transfected with Cx43 alone (Fig. 6B). In contrast, co-transfection with HA–NEDD4-C867A did not significantly reduce the Cx43 protein levels (Fig. 6A,B). Collectively, these data indicate that ectopic overexpression of NEDD4 in HeLa cells results in loss of gap junctions and reduced Cx43 protein levels in a process that requires a functional HECT domain.

To determine the effect of overexpression of HA–NEDD4-WT or HA–NEDD4-C867A on the Cx43 ubiquitylation status, HeLa-CCL2 cells were transfected with Cx43 alone or with Cx43 in combination with HA–NEDD4-WT or HA–NEDD4-C867A, followed by immunoprecipitation and western blotting. The overall Cx43 ubiquitylation status increased by ∼60% in response to overexpression of HA–NEDD4-WT, but not HA–NEDD4-C867A, compared with that in control cells (Fig. 6C,D).

NEDD4 promotes loss of gap junctions in C33A cells

Next, we aimed to examine whether ectopic overexpression of NEDD4 results in loss of gap junctions in a cervical carcinoma cell line that expresses Cx43 endogenously. To this end, we used the C33A cell line as a model system, since it has previously been shown to express relatively high levels of Cx43, a portion of which is assembled into gap junctions at the plasma membrane (Aasen et al., 2003). To our knowledge, a detailed ultrastructural analysis of the endocytic pathway followed by Cx43 in cervical cancer cells that express Cx43 endogenously has not previously been performed. Therefore, we first analyzed the subcellular localization of Cx43 in C33A cells by immunoelectron microscopy. As expected, Cx43 formed gap junctions between adjacent C33A cells (Fig. 7A). Cx43 was also often organized as annular gap junctions (Fig. 7B,C), or localized in multivesicular endosomes, indicating that degradation of Cx43 in these cells involves the endolysosomal pathway (Fig. 7D). In a manner similar to that previously observed in IAR20 cells (Leithe et al., 2006a) and HeLa-Cx43 cells (Fig. 1H), annular gap junctions sometimes appeared to be in the process of undergoing a transformation from a double-membrane vesicular structure into a multivesicular endosome, displaying small intraluminal vesicles and an apparent disruption of the double-membrane structure (Fig. 7B).

Confocal fluorescence microscopy confirmed that part of the Cx43 pool in the C33A cells was organized as gap junctions between adjacent cells (Fig. 7E). Furthermore, a substantial fraction of Cx43 also localized in intracellular structures, in accordance with the immunoelectron microscopy analysis (Fig. 7E). Similar to what was observed in HeLa-Cx43 cells, transfection of HA–NEDD4-WT in C33A cells resulted in a nearly complete loss of gap junctions

Journal of Cell Science (2017) 130, 2867-2882 doi:10.1242/jcs.202408

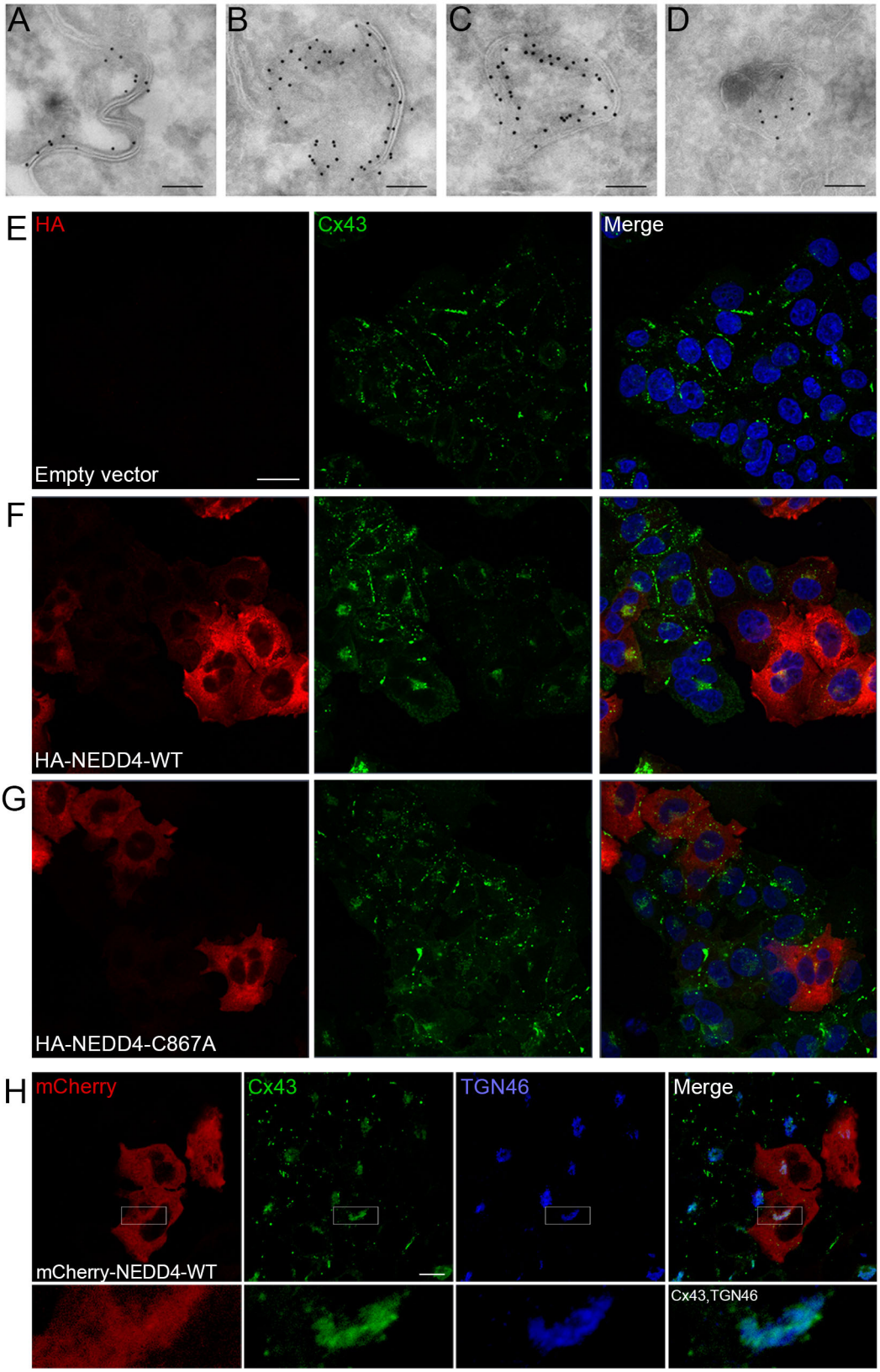

Fig. 7. Effect of ectopic overexpression of NEDD4 on Cx43 subcellular localization in C33A cells. (A–D) C33A cells were fixed for immunoelectron microscopy, and ultrathin cryosections were labeled for Cx43 by using anti-Cx43 antibodies, followed by incubation with 10 nm Protein-A–gold particles. (A) Cx43 staining in gap junction between two adjacent cells. (B,C) Cx43 staining in annular gap junctions. (D) Cx43 staining in a multivesicular endosome. Scale bars: 100 nm. (E–G) C33A cells were transfected with empty vector (E), HA–NEDD4-WT (F) or HA–NEDD4-C867A (G) for 48 h. Cx43 (green) and HA (red) were visualized by confocal fluorescence microscopy. Scale bar: 20 µm. (H) C33A cells were transfected with mCherry–NEDD4-WT. Cx43 (green) and TGN46 (blue) were visualized by confocal fluorescence microscopy. Scale bar: 10 µm.

Journal of Cell Science (2017) 130, 2867-2882 doi:10.1242/jcs.202408

between adjacent cells (Fig. 7F). Moreover, cells transfected with HA–NEDD4-WT displayed very low levels of Cx43 staining in intracellular vesicular structures, except for some Cx43 staining observed in vesicular compartments localized in the perinuclear area. This Cx43 pool may, at least partly, represent newly synthesized Cx43 localized in the secretory pathway that is not subjected to NEDD4-mediated ubiquitylation and degradation. To investigate the subcellular localization of this Cx43 pool in further detail, C33A cells were transfected with plasmids encoding NEDD4-WT tagged with the red fluorescent protein mCherry (mCherry–NEDD4-WT). Cells were then co-stained against Cx43 and the trans-Golgi network marker TGN46 (also known as TGOLN2) and analyzed by confocal fluorescence microscopy. This analysis revealed that the pool of perinuclear Cx43 observed in cells overexpressing NEDD4-WT partly colocalized with TGN46 (Fig. 7H). On the basis of these observations, we conclude that the Cx43 pool that is not downregulated in C33A cells overexpressing NEDD4 represents, at least in part, newly synthesized Cx43 localized in the secretory pathway.

Similar to what is observed in HeLa-Cx43 cells, transfecting C33A cells with HA–NEDD4-C867A did not have any apparent effect on the gap junction size or the overall intensity of subcellular Cx43 staining (Fig. 7G). Collectively, these data indicate that ectopic overexpression of NEDD4, but not NEDD4 containing an inactive HECT domain, causes loss of gap junctions and reduced Cx43 staining in intracellular compartments in C33A cells.

The NEDD4-induced loss of Cx43 expression and gap junctions could be due to either reduced Cx43 synthesis or increased Cx43 degradation. To provide a better understanding of the mechanisms involved in the NEDD4-induced loss of Cx43 gap junctions, we investigated the effect of lysosomal and proteasomal inhibitors on this process. Proteasomal inhibitors have previously been shown to counteract Cx43 gap junction endocytosis (Girao and Pereira, 2007; Laing et al., 1997; Leithe et al., 2009; Musil et al., 2000; Qin et al., 2003; VanSlyke and Musil, 2005). The proteasomal inhibitor MG132 was found to strongly counteract the HA–NEDD4-induced loss of Cx43 gap junctions in C33A cells, as determined by confocal fluorescence microscopy (Fig. 8A). The lysosomal inhibitor chloroquine was also found to strongly prevent the loss of Cx43 staining in C33A cells induced by ectopic overexpression of HA–NEDD4 (Fig. 8A). Under these conditions, Cx43 accumulated in intracellular vesicular compartments. In order to more precisely define these structures, we investigated whether they represented early and late endosomes or lysosomes. To this end, C33A cells were transfected with plasmids encoding mCherry–NEDD4-WT and treated with chloroquine as described above. The cells were then co-stained for Cx43 and EEA1 or LAMP1. As determined by confocal fluorescence microscopy, the Cx43-positive vesicles observed under these conditions were frequently positive for EEA1 or LAMP1 (Fig. 8B). Taken together, these data suggest that the NEDD4-induced loss of Cx43 gap junctions in C33A cells is due to increased Cx43 gap junction endocytosis and lysosomal degradation.

DISCUSSION

Cx43 has been demonstrated to act as a tumor suppressor in various human tissue types (Aasen et al., 2016). Moreover, the level of connexins and gap junctions in tumor cells may affect their response to radiation exposure and chemotherapeutic agents (Prise and O'Sullivan, 2009). Cx43 is frequently dysregulated at the post-translational level in cancer cells, resulting in loss of gap junctions between cells (Mesnil et al., 2005). However, the post-translational mechanisms involved in the loss of Cx43 and gap junctions during carcinogenesis have remained poorly understood. Protein ubiquitylation is a highly regulated process (Hoeller et al., 2006). Several of the components of the ubiquitin system have been shown to play important roles in cancer pathogenesis (Hoeller et al., 2006). Among these is the E3 ubiquitin ligase NEDD4, a member of the HECT family of E3 ubiquitin ligases (Zou et al., 2015). In the present work, we show that NEDD4 controls the Cx43 protein levels in HeLa cells, both under basal conditions and in response to TPA treatment. We also demonstrate that ectopic overexpression of NEDD4, but not a catalytically inactive version of NEDD4, results in loss of gap junctions in both HeLa and C33A cells. Taken together, the data provide new insights into the molecular mechanisms involved in the regulation of the Cx43 protein level and gap junction size. The findings may have important implications for our understanding of the post-translational mechanisms involved in loss of gap junctions during cancer development.

Previous studies have identified a role of autophagy in the degradation of Cx43 in HeLa cells under basal conditions (Carette et al., 2015; Fong et al., 2012). In the present study, we provide super-resolution and immunoelectron microscopy evidence that, in addition to the autophagosomal pathway, the endolysosomal pathway is involved in the degradation of Cx43 in HeLa-Cx43 cells under basal conditions. Our data further demonstrate that exposure of HeLa-Cx43 cells to TPA induces Cx43 degradation by promoting its sorting along the endolysosomal pathway. Moreover, the finding that Cx43 frequently localizes in multivesicular endosomes in C33A cells under basal conditions raises the possibility that aberrant regulation of the endocytosis and endolysosomal sorting of Cx43 may be causally involved in mediating the loss of gap junctions during cervical cancer pathogenesis. The formation of Cx43-enriched multivesicular endosomes, as observed by immunoelectron microscopy, is likely to involve a fusion process between annular gap junctions and multivesicular endosomes. In line with this notion, Cx43-positive vesicular structures often appeared to be in the process of undergoing fusion with EEA1-positive vesicles, as determined by three-dimensional reconstruction of super-resolution images. Following the trafficking of Cx43 to multivesicular endosomes, the endosomes may fuse with lysosomes, resulting in degradation of Cx43. Alternatively, Cx43 might undergo recycling from the multivesicular endosomes to the plasma membrane. In accordance with this model, Cx43 has been shown to be transported to early endosomes during the early phases of mitosis and is thought to undergo recycling to the plasma membrane in the late phases (Boassa et al., 2010; Fykerud et al., 2016; Vanderpuye et al., 2016). Recently, Graham and colleagues demonstrated that ectopic overexpression of human papillomavirus (HPV) E6 oncoprotein in C33A cells results in redistribution of Cx43 from the plasma membrane to the cytoplasm and reduced Cx43 levels (Sun et al., 2015). In future studies, it would be interesting to elucidate whether the E6-induced loss of Cx43 expression involves increased Cx43 ubiquitylation and sorting via the endolysosomal pathway, similar to what is observed in response to NEDD4 overexpression.

Serum starvation has been shown to result in increased endocytosis and autophagy-mediated degradation of Cx43, which is associated with enhanced Cx43 ubiquitylation (Bejarano et al., 2012; Lichtenstein et al., 2011). The autophagy-mediated degradation of Cx43 in response to serum starvation has been shown to be mediated by NEDD4 (Bejarano et al., 2012). However, the role of NEDD4 in the regulation of Cx43 protein levels under basal conditions is less well

Journal of Cell Science (2017) 130, 2867-2882 doi:10.1242/jcs.202408

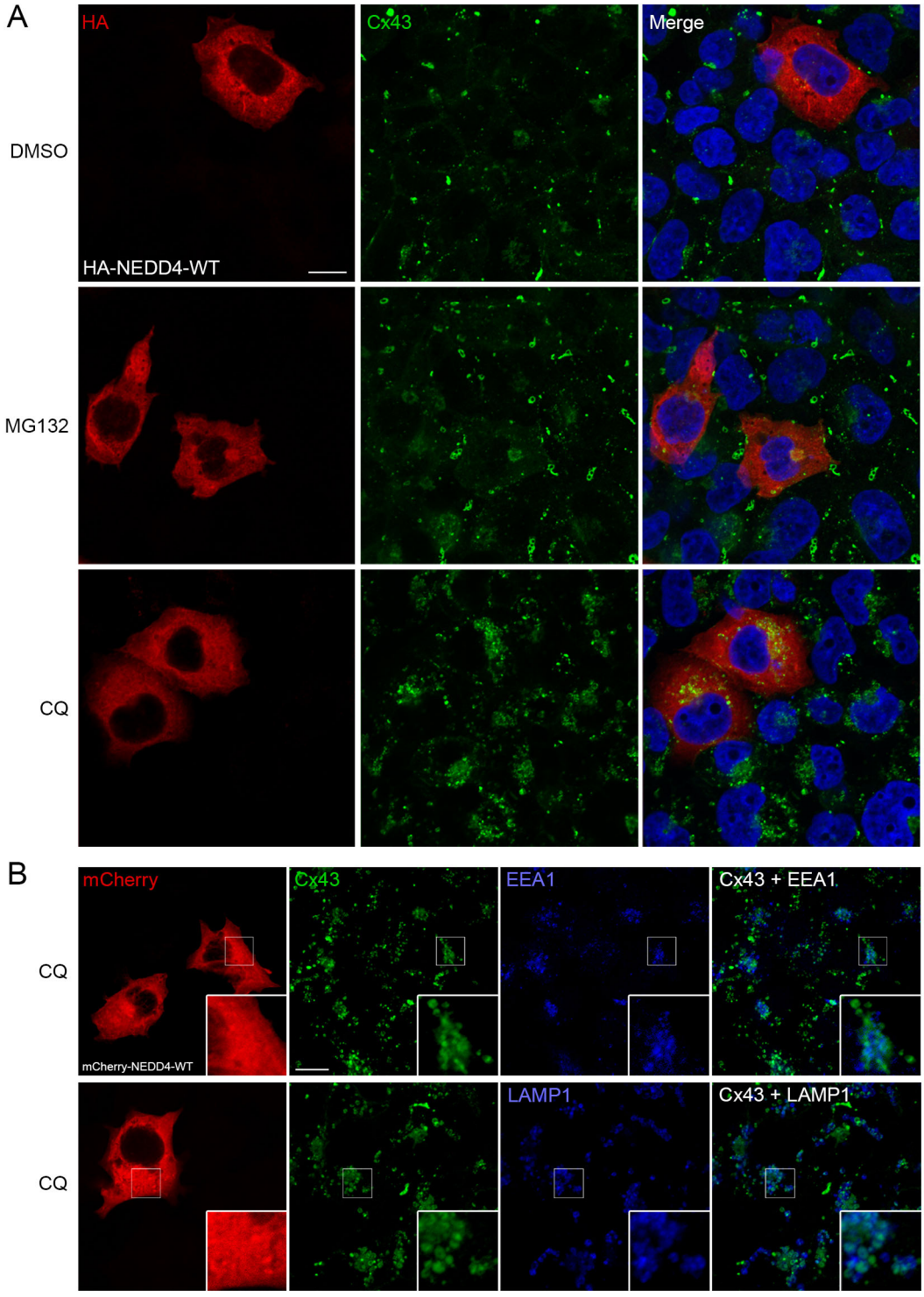

Fig. 8. Effect of lysosomal and proteasomal inhibitors on the NEDD4-induced loss of Cx43. (A) C33A cells were transfected with HA–NEDD4-WT for 48 h. The cells were treated with DMSO (solvent), MG132 (10 µM) or chloroquine (CQ; 100 µM) for 5 h, as indicated. Cx43 (green) and HA (red) were visualized by confocal fluorescence microscopy. (B) C33A cells were transfected with mCherry–NEDD4-WT for 48 h. The cells were treated with chloroquine (100 µM) for 5 h. Cx43 (green), EEA1 (blue, upper panel), and LAMP1 (blue, lower panel) were visualized by confocal fluorescence microscopy. Scale bars: 10 µm.

understood. Depletion of NEDD4 in WB-F344 rat liver cells (Leykauf et al., 2006) and Cos-7 monkey kidney cells (Girao et al., 2009) has been reported to result in accumulation of gap junctions between cells. However, in neither of these cell lines did depletion of NEDD4 affect the overall cellular Cx43 protein level. To our knowledge, the role of NEDD4 in regulating Cx43 protein levels and gap junctions in human cell lines had not been examined. Here, we report that depletion of NEDD4 in HeLa-Cx43 cells results in increased Cx43 protein levels and enlarged gap junctions. Our data further indicate that NEDD4 is involved in mediating the TPA-induced endocytosis and degradation of Cx43 in HeLa-Cx43 cells. Taken together, the data suggest that NEDD4 is involved in mediating the endolysosomal degradation of

Cx43 under basal conditions and in response to PKC activation, thus revealing a novel Cx43 degradation pathway that is regulated by NEDD4 (Fig. S8).

In this study, we demonstrate that ectopic overexpression of NEDD4 in HeLa or C33A cells results in loss of gap junctions and reduced Cx43 protein levels in a process that requires a functional HECT domain. To our knowledge, these findings represent the first proof of principle that overexpression of an oncogenic E3 ubiquitin ligase in human cancer cells causes downregulation of gap junctions. In C33A cells, the ectopic overexpression of NEDD4 also resulted in a strong reduction in Cx43 staining in intracellular vesicles, except for some staining in vesicular compartments localized in the perinuclear area. Our data suggest that at least part of this Cx43 pool represents Cx43 localized in the secretory pathway, since it partly colocalized with the trans-Golgi network marker TGN46. These findings suggest that the newly synthesized Cx43 localized in the secretory pathway may not be targeted for NEDD4-mediated degradation as efficiently as the Cx43 pool localized at the plasma membrane or in endolysosomal compartments. The ability of NEDD4 to interact with Cx43 may depend on the Cx43 phosphorylation status (Leykauf et al., 2006; Spagnol et al., 2016). Thus, a possible explanation for the observation that the Cx43 pool localized in the secretory pathway is not downregulated in response to NEDD4 overexpression may be that this Cx43 pool has not yet been subjected to the specific phosphorylation events that are required for binding NEDD4.

The present study indicates that a subpool of Cx43 is ubiquitylated under basal conditions in HeLa-Cx43 cells and that Cx43 ubiquitylation is increased in response to TPA treatment in a PKC-dependent manner. Our data further suggest that depletion of NEDD4 does not have major effects on the overall Cx43 ubiquitylation status, as determined by immunoprecipitation and western blotting. A possible explanation for this observation is that NEDD4 may catalyze the ubiquitylation of one or only a few lysine residues in Cx43, and that counteracting the ubiquitylation of these lysine residues by depletion of NEDD4 is not sufficient to observe an effect on the overall Cx43 ubiquitylation as determined by immunoprecipitation and western blotting. In future experiments, it will be important to precisely define which lysine residue(s) in Cx43 are ubiquitylated by NEDD4 by mass spectrometry analysis.

In conclusion, the present study provides new insights into the role of the ubiquitin system in modulating gap junction size and Cx43 degradation. The study also represents the first evidence that overexpression of an oncogenic E3 ubiquitin ligase in cancer cells causes loss of gap junctions. Given that proto-oncogenic E3 ubiquitin ligases, including NEDD4, are potential targets in cancer therapy, these findings may have considerable future clinical relevance.

MATERIALS AND METHODS

Cell culture

HeLa-CCL2 and C33A cells were obtained from the ATCC. HeLa cells stably transfected with Cx43 (HeLa-Cx43) were a gift from Professor Klaus Willecke (University of Bonn, Germany) and have been described previously (Elfgang et al., 1995). Cells were grown on 35-mm or 100-mm Petri dishes in Dulbecco's modified Eagle's medium (DMEM) supplemented with 10% (v/v) fetal bovine serum (FBS) (Gibco BRL Life Technologies, Inchinnan, UK) and 1% L-glutamine Sigma-Aldrich (St Louis, MO).

Reagents and antibodies

TPA, cycloheximide, chloroquine, MG132, and GF109203X were obtained from Sigma-Aldrich. Anti-Cx43 antibodies were obtained by injecting rabbits with a synthetic peptide consisting of the 20 C-terminal amino acids of Cx43 (western blotting, 1:5000; immunofluorescence 1:500; immunoprecipitation 1:10) (Rivedal et al., 1994). Mouse anti-ubiquitin (P4D1; 1:1500) antibodies were obtained from Covance (Berkeley, CA). Mouse anti-β-actin (A2228; 1:5000) antibodies were purchased from Sigma-Aldrich. Mouse anti-EEA1 (610456; 1:500) antibodies were from BD Transduction Laboratories (Franklin Lakes, NJ). Rabbit anti-NEDD4 (ab14592; 1:5000) and rabbit anti-TGN46 (ab50595; 1:100) antibodies were from Abcam (Cambridge, UK). Mouse anti-HA antibodies (6E2; western blotting 1:1000; immunofluorescence 1:100) were obtained from Cell Signaling Technology (Danvers, MA). Mouse anti-LAMP1 (H4A3; 1:100) antibodies were from DSHB (Iowa City, IA). Alexa Fluor 405-conjugated goat anti-mouse-IgG (A31553; 1:1000), Alexa Fluor 488-conjugated goat anti-rabbit-IgG (A11034; 1:1000), Alexa Fluor 555-conjugated goat anti-mouse-IgG (A21424, 1:1000), and Alexa Fluor 555-conjugated WGA (W32464) were from Thermo Fisher Scientific (Waltham, MA). Horseradish peroxidase-conjugated goat anti-rabbit-IgG secondary antibodies (170-6515; 1:2000) were from Bio-Rad (Hercules, CA). Horseradish peroxidase-conjugated donkey anti-mouse-IgG antibodies (715-035-150; 1:2000) were obtained from Jackson Immunoresearch Laboratories (West Grove, PA). Donkey anti-mouse IRDye 680RD (926-68072; 1:15000) and Donkey anti-rabbit IRDye 800CW (926-32213; 1:15000) were obtained from Li-COR Biotechnology (Lincoln, NE). Rabbit IgG was from Cell Signaling Technology. Protein-A–Sepharose CL-4B was from GE Healthcare Life Sciences (Chicago, IL). Protein-A–gold was obtained from University Medical Center Utrecht (Utrecht, The Netherlands). Phosphatase inhibitor cocktail II (P5726), phosphatase inhibitor cocktail III (P0044) and protease inhibitor cocktail (P8340) were from Sigma-Aldrich.

DNA and siRNA transfection

The expression plasmid pcDNA I/Neo (Invitrogen, San Diego, CA) encoding Cx43 was a kind gift from Klaus Willecke (University of Bonn, Germany), and has been described previously (Elfgang et al., 1995). pCI-HA-NEDD4-WT and pCI-HA-NEDD4-C867A were Addgene plasmids #27002 and #26999 (deposited by Joan Massagué; Gao et al., 2009). pCl-mCherry-NEDD4-WT was Addgene plasmid #38316 (deposited by Quan Lu; Nabhan et al., 2010). Cells grown on 35-mm Petri dishes were transfected with plasmids 24 h after seeding by using Lipofectamine 2000 reagent from Thermo Fisher Scientific according to the recommendations of the manufacturer, as described previously (Kjenseth et al., 2012). The siRNA oligonucleotide targeting *NEDD4* (Hs_NEDD4_8) was obtained from Qiagen, and had the following sequence: 5′-GGAGAAUUAUGGGUGU-CAATT-3′. The siRNA control construct was Stealth RNAi Negative Control (Medium GC) from Thermo Fisher Scientific. Cells were transfected with siRNA twice over a period of 96 h, by using Lipofectamine 2000 at a final concentration of 80 nM.

Immunoprecipitation

Immunoprecipitation of Cx43 was performed as described previously (Kjenseth et al., 2012).

Western blotting

Western blotting was performed as described previously (Kjenseth et al., 2012). Samples were separated by 7.5% SDS-PAGE and transferred onto nitrocellulose membranes for chemiluminescence detection or to low-fluorescence PVDF membranes for fluorescence detection. For chemiluminescent detection, the membranes were developed by using Lumiglo (EMD Millipore, Billerica, MA, USA) or SuperSignal West Dura Extended Duration Substrate (Thermo Fisher Scientific), and imaged with the ChemiDoc XRS+ System (Bio-Rad). For fluorescence detection, secondary antibodies were detected by using the Odyssey imaging system. Bands were quantified with ImageJ 1.48v.

Confocal fluorescence microscopy

Cells grown in a monolayer were fixed with 4% formaldehyde in PBS for 15 min at room temperature and rinsed in PBS. Cells to be stained with anti-Cx43 alone or in combination with anti-EEA1, anti-HA or anti-TGN46 were

permeabilized with 0.1% Triton X-100 in PBS. The cells were incubated with primary antibodies diluted in PBS containing 5% (w/v) dry milk powder and 0.1% Tween 20 overnight. Cells to be co-stained with anti-LAMP1 and anti-Cx43 antibodies were permeabilized with 0.05% (w/v) saponin in PBS. The cells were then incubated with primary antibodies diluted in PBS containing 0.05% (w/v) saponin overnight. The cells were washed with PBS and incubated for 1 h with secondary antibodies conjugated to Alexa Fluor 405, Alexa Fluor 488 and/or Alexa Fluor 555 in different combinations, depending on which primary antibodies were used. In some experiments, cells were incubated with WGA conjugated to Alexa Fluor 555 diluted in Hank's balanced salt solution (HBSS) to a final concentration of 5 µg/ml for 10 min, in order to stain the plasma membrane. Nuclei were stained with Hoechst 33342 (10 µg/ml in PBS). All samples were mounted using ProLong Gold Antifade Mountant (ThermoFisher Scientific) on object slides. The cells were analyzed with an LSM 710 META confocal microscope (Carl Zeiss Inc., Oberkochen, Germany) equipped with a Plan Apochromat 63×1.4 NA oil immersion objective (Carl Zeiss Inc.). Images were acquired with the ZEN 2009 edition software and processed with Adobe Photoshop CS4.

SIM

HeLa-Cx43 cells were fixed with 4% formaldehyde diluted in PBS. Immunostaining and mounting of the samples were performed as described above. Three-dimensional SIM was performed on a Deltavision OMX V4 microscope (Applied Precision, Inc., Issaquah, WA, USA) equipped with an Olympus 60×1.42 NA Plan Apochromat objective; 405 nm, 445 nm, 488 nm, 568 nm, and 642 nm laserlines; and three cooled sCMOS cameras. *z*-stacks covering the whole cell were recorded, with a *z*-spacing of 125 nm. For each focal plane, 15 raw images (five phases for three different angular orientations of the illumination pattern) were captured. Super-resolution images were reconstructed, aligned, and processed for presentation by using Softworx software (Applied Precision, Inc.). IMARIS software was used for three-dimensional reconstruction. IMARIS software was used for three-dimensional reconstruction, as described previously (Malerod et al., 2011).

Immunoelectron microscopy

Untreated cells or cells treated with TPA as indicated were fixed and prepared for immunoelectron microscopy as described previously (Leithe et al., 2006a). Ultrathin cryosections were cut at −110°C with a diamond knife in an Ultracut microtome (Leica), collected with a drop of a 1:1 mixture of 2.3 M sucrose and 2% methyl cellulose, and thawed at room temperature. Sections were transferred to formvar- and carbon-coated grids and labeled with anti-Cx43 antibodies, followed by Protein-A–gold conjugates as described previously (Slot et al., 1991). The labeled cryosections were examined with a JEM 1230 (JEOL) electron microscope. For quantification of the number of Cx43-positive multivesicular bodies per cell section, 100 cell sections of untreated and TPA-treated HeLa-Cx43 cells obtained from two independent experiments were analyzed. Multivesicular bodies containing at least one immunogold particle were defined as Cx43-positive. For visualization of multivesicular endosomes in cells embedded in Lowicryl, samples were prepared as described previously by Kukulski et al. (2012).

Statistical analysis

Data were statistically analyzed by using SigmaPlot 12.5. Statistically significant differences between groups were determined by one-way ANOVA with post hoc analysis using Student–Newman–Keuls multiple comparison test.

Acknowledgements

We are grateful to Marianne Smestad and Linn Kymre (Oslo University Hospital) for excellent technical assistance.

Competing interests

The authors declare no competing or financial interests.

Author contributions

Conceptualization: M.Z.T., C.H.B., T.A.F., L.M.K., N.L.R., V.S., A.B., R.A.L., E.L.; Methodology: M.Z.T., C.H.B., T.A.F., L.M.K., N.L.R., P.W.E., Z.Y., V.S., A.B., E.L.; Validation: M.Z.T., C.H.B., T.A.F., L.M.K., N.L.R., P.W.E., Z.Y., V.S., A.B.; Formal analysis: M.Z.T., C.H.B., T.A.F., L.M.K., N.L.R., P.W.E., Z.Y., V.S., A.B., R.A.L., E.L.; Investigation: M.Z.T., C.H.B., T.A.F., L.M.K., N.L.R., Z.Y., V.S., A.B., E.L.; Resources: R.A.L., E.L.; Writing - original draft: M.Z.T., C.H.B., T.A.F., L.M.K, N.L.R., E.L.; Writing - review & editing: M.Z.T., C.H.B., T.A.F., L.M.K., N.L.R., P.W.E., V.S., A.B., R.A.L., E.L.; Visualization: M.Z.T., L.M.K., A.B., R.A.L., E.L.; Supervision: E.L.; Project administration: E.L.; Funding acquisition: R.A.L., E.L.

Funding

This work was supported by Kreftforeningen (Norwegian Cancer Society) (709125 to E.L.); Norges Forskningsråd (Research Council of Norway through its Centres of Excellence funding scheme) (project number 179571 to R.A.L, A.B., V.S., and E.L.), and Stiftelsen Kristian Gerhard Jebsen (to R.A.L.).

Supplementary information

Supplementary information available online at http://jcs.biologists.org/lookup/doi/10.1242/jcs.202408.supplemental

References

Aasen, T., Hodgins, M. B., Edward, M. and Graham, S. V. (2003). The relationship between connexins, gap junctions, tissue architecture and tumour invasion, as studied in a novel in vitro model of HPV-16-associated cervical cancer progression. *Oncogene* **22**, 7969-7980.

Aasen, T., Graham, S. V., Edward, M. and Hodgins, M. B. (2005). Reduced expression of multiple gap junction proteins is a feature of cervical dysplasia. *Mol. Cancer* **4**, 31.

Aasen, T., Mesnil, M., Naus, C. C., Lampe, P. D. and Laird, D. W. (2016). Gap junctions and cancer: communicating for 50 years. *Nat. Rev. Cancer* **16**, 775-788.

Amodio, N., Scrima, M., Palaia, L., Salman, A. N., Quintiero, A., Franco, R., Botti, G., Pirozzi, P., Rocco, G., De, R. N. et al. (2010). Oncogenic role of the E3 ubiquitin ligase NEDD4-1, a PTEN negative regulator, in non-small-cell lung carcinomas. *Am. J. Pathol.* **177**, 2622-2634.

Asamoto, M., Oyamada, M., el Aoumari, A., Gros, D. and Yamasaki, H. (1991). Molecular mechanisms of TPA-mediated inhibition of gap-junctional intercellular communication: evidence for action on the assembly or function but not the expression of connexin 43 in rat liver epithelial cells. *Mol. Carcinog.* **4**, 322-327.

Bager, Y., Kenne, K., Krutovskikh, V., Mesnil, M., Traub, O. and Wärngård, L. (1994). Alteration in expression of gap junction proteins in rat liver after treatment with the tumour promoter 3,4,5,3',4'-pentachlorobiphenyl. *Carcinogenesis* **15**, 2439-2443.

Basheer, W. A., Harris, B. S.,, Mentrup, H. L., Abreha, M., Thames, E. L., Lea, J. B., Swing, D. A., Copeland, N. G., Jenkins, N. A., Price, R. L. et al. (2015). Cardiomyocyte-specific overexpression of the ubiquitin ligase Wwp1 contributes to reduction in Connexin 43 and arrhythmogenesis. *J. Mol. Cell. Cardiol.* **88**, 1-13.

Bejarano, E., Girao, H., Yuste, A., Patel, B., Marques, C., Spray, D. C., Pereira, P. and Cuervo, A. M. (2012). Autophagy modulates dynamics of connexins at the plasma membrane in a ubiquitin-dependent manner. *Mol. Biol. Cell* **23**, 2156-2169.

Bernassola, F., Karin, M., Ciechanover, A. and Melino, G. (2008). The HECT family of E3 ubiquitin ligases: multiple players in cancer development. *Cancer Cell* **14**, 10-21.

Berthoud, V. M., Rook, M. B., Traub, O., Hertzberg, E. L. and Saez, J. C. (1993). On the mechanisms of cell uncoupling induced by a tumor promoter phorbol ester in clone 9 cells, a rat liver epithelial cell line. *Eur. J. Cell Biol.* **62**, 384-396.

Boase, N. A. and Kumar, S. (2015). NEDD4: The founding member of a family of ubiquitin-protein ligases. *Gene* **557**, 113-122.

Boassa, D., Solan, J. L., Papas, A., Thornton, P., Lampe, P. D. and Sosinsky, G. E. (2010). Trafficking and recycling of the connexin43 gap junction protein during mitosis. *Traffic* **11**, 1471-1486.

Carette, D., Gilleron, J., Denizot, J.-P., Grant, K., Pointis, G. and Segretain, D. (2015). New cellular mechanisms of gap junction degradation and recycling. *Biol. Cell* **107**, 218-231.

Catarino, S. M., Ramalho, J. S., Marques, C., Pereira, P. C. and Girão H. (2011). Ubiquitin-mediated internalization of Connexin43 is independent on the canonical endocytic tyrosine-sorting signal. *Biochem. J.* **437**, 255-267.

Chen, V. C., Kristensen, A. R., Foster, L. J. and Naus, C. C. (2012). Association of connexin43 with E3 ubiquitin ligase TRIM21 reveals a mechanism for gap junction phosphodegron control. *J. Proteome Res.* **11**, 6134-6146.

Dunn, C. A., Su, V., Lau, A. F. and Lampe, P. D. (2012). Activation of Akt, not connexin 43 protein ubiquitination, regulates gap junction stability. *J. Biol. Chem.* **287**, 2600-2607.

Eide, P. W., Cekaite, L., Danielsen, S. A., Eilertsen, I. A., Kjenseth, A., Fykerud, T. A., Ågesen, T. H., Bruun, J., Rivedal, E., Lothe, R. A. et al. (2013). NEDD4 is overexpressed in colorectal cancer and promotes colonic cell growth independently of the PI3K/PTEN/AKT pathway. *Cell. Signal.* **25**, 12-18.

Elfgang, C., Eckert, R., Lichtenberg-Fraté, H., Butterweck, A., Traub, O. Klein, R. A., Hulser, D. F. and Willecke, K. (1995). Specific permeability and selective formation of gap junction channels in connexin-transfected HeLa cells. *J. Cell Biol.* **129**, 805-817.

Enomoto, T., Martel, N., Kanno, Y. and Yamasaki, H. (1984). Inhibition of cell communication between Balb/c 3T3 cells by tumor promoters and protection by cAMP. *J. Cell Physiol.* **121**, 323-333.
Falk, M. M., Kells, R. M. and Berthoud, V. M. (2014). Degradation of connexins and gap junctions. *FEBS Lett.* **588**, 1221-1229.
Fong, J. T., Kells, R. M., Gumpert, A. M., Marzillier, J. Y., Davidson, M. W. and Falk, M. M. (2012). Internalized gap junctions are degraded by autophagy. *Autophagy* **8**, 794-811.
Fykerud, T. A., Kjenseth, A., Schink, K. O., Sirnes, S., Bruun, J., Omori, Y., Brech, A., Rivedal, E. and Leithe, E. (2012). Smad ubiquitination regulatory factor-2 controls gap junction intercellular communication by modulating endocytosis and degradation of connexin43. *J. Cell Sci.* **125**, 3966-3976.
Fykerud, T. A., Knudsen, L. M., Totland, M. Z., Sørensen, V., Dahal-Koirala, S., Lothe, R. A., Brech, A. and Leithe, E. (2016). Mitotic cells form actin-based bridges with adjacent cells to provide intercellular communication during rounding. *Cell Cycle* **15**, 2943-2957.
Gao, S., Alarcón, C., Sapkota, G., Rahman, S., Chen, P.-Y., Goerner, N., Macias, M. J., Erdjument-Bromage, H., Tempst, P. and Massagué, J. (2009). Ubiquitin ligase Nedd4L targets activated Smad2/3 to limit TGF-beta signaling. *Mol. Cell* **36**, 457-468.
Girao, H. and Pereira, P. (2007). The proteasome regulates the interaction between Cx43 and ZO-1. *J. Cell. Biochem.* **102**, 719-728.
Girão, H., Catarino, S. and Pereira, P. (2009). Eps15 interacts with ubiquitinated Cx43 and mediates its internalization. *Exp. Cell Res.* **315**, 3587-3597.
Guan, X. and Ruch, R. J. (1996). Gap junction endocytosis and lysosomal degradation of connexin43-P2 in WB-F344 rat liver epithelial cells treated with DDT and lindane. *Carcinogenesis* **17**, 1791-1798.
Hesketh, G. G., Shah, M. H., Halperin, V. L., Cooke, C. A., Akar, F. G., Yen, T. E., Kass, D. A., Machamer, C. E., Van Eyk, J. E. and Tomaselli, G. F. (2010). Ultrastructure and regulation of lateralized connexin43 in the failing heart. *Circ. Res.* **106**, 1153-1163.
Hoeller, D., Hecker, C.-M. and Dikic, I. (2006). Ubiquitin and ubiquitin-like proteins in cancer pathogenesis. *Nat. Rev. Cancer* **6**, 776-788.
Huibregtse, J. M., Scheffner, M., Beaudenon, S. and Howley, P. M. (1995). A family of proteins structurally and functionally related to the E6-AP ubiquitin-protein ligase. *Proc. Natl. Acad. Sci. USA* **92**, 2563-2567.
Johnson, K. E., Mitra, S., Katoch, P., Kelsey, L. S., Johnson, K. R. and Mehta, P. P. (2013). Phosphorylation on Ser-279 and Ser-282 of connexin43 regulates endocytosis and gap junction assembly in pancreatic cancer cells. *Mol. Biol. Cell* **24**, 715-733.
King, T. J., Fukushima, L. H., Donlon, T. A., Hieber, A. D., Shimabukuro, K. A. and Bertram, J. S. (2000a). Correlation between growth control, neoplastic potential and endogenous connexin43 expression in HeLa cell lines: implications for tumor progression. *Carcinogenesis* **21**, 311-315.
King, T. J., Fukushima, L. H., Hieber, A. D., Shimabukuro, K. A., Sakr, W. A. and Bertram, J. S. (2000b). Reduced levels of connexin43 in cervical dysplasia: inducible expression in a cervical carcinoma cell line decreases neoplastic potential with implications for tumor progression. *Carcinogenesis* **21**, 1097-1109.
Kjenseth, A., Fykerud, T. A., Sirnes, S., Bruun, J., Yohannes, Z., Kolberg, M., Omori, Y., Rivedal, E. and Leithe, E. (2012). The gap junction channel protein connexin 43 is covalently modified and regulated by SUMOylation. *J. Biol. Chem.* **287**, 15851-15861.
Krutovskikh, V. A., Mesnil, M., Mazzoleni, G. and Yamasaki, H. (1995). Inhibition of rat liver gap junction intercellular communication by tumor-promoting agents in vivo. Association with aberrant localization of connexin proteins. *Lab. Invest.* **72**, 571-577.
Kukulski, W., Schorb, M., Kaksonen, M. and Briggs, J. A. G. (2012). Plasma membrane reshaping during endocytosis is revealed by time-resolved electron tomography. *Cell.* **150**, 508-520.
Laing, J. G. and Beyer, E. C. (1995). The gap junction protein connexin43 is degraded via the ubiquitin proteasome pathway. *J. Biol. Chem.* **270**, 26399-26403.
Laing, J. G., Tadros, P. N., Westphale, E. M. and Beyer, E. C. (1997). Degradation of connexin43 gap junctions involves both the proteasome and the lysosome. *Exp. Cell Res.* **236**, 482-492.
Laird, D. W. (2006). Life cycle of connexins in health and disease. *Biochem. J.* **394**, 527-543.
Lampe, P. D. (1994). Analyzing phorbol ester effects on gap junctional communication: a dramatic inhibition of assembly. *J. Cell Biol.* **127**, 1895-1905.
Leithe, E. (2016). Regulation of connexins by the ubiquitin system: Implications for intercellular communication and cancer. *Biochim. Biophys. Acta* **1865**, 133-146.
Leithe, E. and Rivedal, E. (2004a). Epidermal growth factor regulates ubiquitination, internalization and proteasome-dependent degradation of connexin43. *J. Cell Sci.* **117**, 1211-1220.
Leithe, E. and Rivedal, E. (2004b). Ubiquitination and down-regulation of gap junction protein connexin-43 in response to 12-O-tetradecanoylphorbol 13-acetate treatment. *J. Biol. Chem.* **279**, 50089-50096.
Leithe, E., Cruciani, V., Sanner, T., Mikalsen, S.-O. and Rivedal, E. (2003). Recovery of gap junctional intercellular communication after phorbol ester treatment requires proteasomal degradation of protein kinase C. *Carcinogenesis* **24**, 1239-1245.
Leithe, E., Brech, A. and Rivedal, E. (2006a). Endocytic processing of connexin43 gap junctions: a morphological study. *Biochem. J.* **393**, 59-67.
Leithe, E., Sirnes, S., Omori, Y. and Rivedal, E. (2006b). Downregulation of gap junctions in cancer cells. *Crit. Rev. Oncog.* **12**, 225-256.
Leithe, E., Kjenseth, A., Sirnes, S., Stenmark, H., Brech, A. and Rivedal, E. (2009). Ubiquitylation of the gap junction protein connexin-43 signals its trafficking from early endosomes to lysosomes in a process mediated by Hrs and Tsg101. *J. Cell Sci.* **122**, 3883-3893.
Leithe, E., Sirnes, S., Fykerud, T., Kjenseth, A. and Rivedal, E. (2012). Endocytosis and post-endocytic sorting of connexins. *Biochim. Biophys. Acta* **1818**, 1870-1879.
Leykauf, K., Salek, M., Bomke, J., Frech, M., Lehmann, W.-D., Dürst, M. and Alonso, A. (2006). Ubiquitin protein ligase Nedd4 binds to connexin43 by a phosphorylation-modulated process. *J. Cell Sci.* **119**, 3634-3642.
Lichtenstein, A., Minogue, P. J., Beyer, E. C. and Berthoud, V. M. (2011). Autophagy: a pathway that contributes to connexin degradation. *J. Cell Sci.* **124**, 910-920.
Malerød, L., Pedersen, N. M., Sem Wegner, C. E., Lobert, V. H., Leithe, E., Brech, A., Rivedal, E., Liestøl, K. and Stenmark, H. (2011). Cargo-dependent degradation of ESCRT-1 as a feedback mechanism to modulate endosomal sorting. *Traffic.* **12**, 1211-1226.
Matesic, D. F., Rupp, H. L., Bonney, W. J., Ruch, R. J. and Trosko, J. E. (1994). Changes in gap-junction permeability, phosphorylation, and number mediated by phorbol ester and non-phorbol-ester tumor promoters in rat liver epithelial cells. *Mol. Carcinog.* **10**, 226-236.
Mesnil, M., Crespin, S., Avanzo, J.-L. and Zaidan-Dagli, M.-L. (2005). Defective gap junctional intercellular communication in the carcinogenic process. *Biochim. Biophys. Acta* **1719**, 125-145.
Mograbi, B., Corcelle, E., Defamie, N., Samson, M., Nebout, M., Segretain, D., Fenichel, P. and Pointis, G. (2003). Aberrant Connexin 43 endocytosis by the carcinogen lindane involves activation of the ERK/mitogen-activated protein kinase pathway. *Carcinogenesis* **24**, 1415-1423.
Murray, A. W. and Fitzgerald, D. J. (1979). Tumor promoters inhibit metabolic cooperation in cocultures of epidermal and 3T3 cells. *Biochem. Biophys. Res. Commun.* **91**, 395-401.
Murray, S. A., Larsen, W. J., Trout, J. and Donta, S. T. (1981). Gap junction assembly and endocytosis correlated with patterns of growth in a cultured adrenocortical tumor cell (SW-13). *Cancer Res.* **41**, 4063-4074.
Musil, L. S., Le, A.-C. N., VanSlyke, J. K. and Roberts, L. M. (2000). Regulation of connexin degradation as a mechanism to increase gap junction assembly and function. *J. Biol. Chem.* **275**, 25207-25215.
Nabhan, J. F., Pan, H. and Lu, Q. (2010). Arrestin domain-containing protein 3 recruits the NEDD4 E3 ligase to mediate ubiquitination of the beta2-adrenergic receptor. *EMBO Rep.* **11**, 605-611.
Naus, C. C. G., Hearn, S., Zhu, D., Nicholson, B. J. and Shivers, R. R. (1993). Ultrastructural analysis of gap junctions in C6 glioma cells transfected with connexin43 cDNA. *Exp. Cell Res.* **206**, 72-84.
Oh, S. Y., Grupen, C. G. and Murray, A. W. (1991). Phorbol ester induces phosphorylation and down-regulation of connexin 43 in WB cells. *Biochim. Biophys. Acta* **1094**, 243-245.
Prise, K. M. and O'Sullivan, J. M. (2009). Radiation-induced bystander signalling in cancer therapy. *Nat. Rev. Cancer* **9**, 351-360.
Qin, H., Shao, Q., Igdoura, S. A., Alaoui-Jamali, M. A. and Laird, D. W. (2003). Lysosomal and proteasomal degradation play distinct roles in the life cycle of Cx43 in gap junctional intercellular communication -deficient and -competent breast tumor cells. *J. Biol. Chem.* **278**, 30005-30014.
Rivedal, E. and Leithe, E. (2005). Connexin43 synthesis, phosphorylation, and degradation in regulation of transient inhibition of gap junction intercellular communication by the phorbol ester TPA in rat liver epithelial cells. *Exp. Cell Res.* **302**, 143-152.
Rivedal, E. and Opsahl, H. (2001). Role of PKC and MAP kinase in EGF- and TPA-induced connexin43 phosphorylation and inhibition of gap junction intercellular communication in rat liver epithelial cells. *Carcinogenesis* **22**, 1543-1550.
Rivedal, E., Yamasaki, H. and Sanner, T. (1994). Inhibition of gap junctional intercellular communication in Syrian hamster embryo cells by TPA, retinoic acid and DDT. *Carcinogenesis* **15**, 689-694.
Ruch, R. J., Trosko, J. E. and Madhukar, B. V. (2001). Inhibition of connexin43 gap junctional intercellular communication by TPA requires ERK activation. *J. Cell Biochem.* **83**, 163-169.
Saez, J. C., Berthoud, V. M., Branes, M. C., Martinez, A. D. and Beyer, E. C. (2003). Plasma membrane channels formed by connexins: their regulation and functions. *Physiol. Rev.* **83**, 1359-1400.
Sirnes, S., Kjenseth, A., Leithe, E. and Rivedal, E. (2009). Interplay between PKC and the MAP kinase pathway in Connexin43 phosphorylation and inhibition of gap junction intercellular communication. *Biochem. Biophys. Res. Commun.* **382**, 41-45.

Slot, J. W., Geuze, H. J., Gigengack, S., Lienhard, G. E. and James, D. E. (1991). Immuno-localization of the insulin regulatable glucose transporter in brown adipose tissue of the rat. *J. Cell Biol.* **113**, 123-135.

Smyth, J. W., Zhang, S.-S., Sanchez, J. M., Lamouille, S., Vogan, J. M., Hesketh, G. G., Hong, T., Tomaselli, G. F. and Shaw, R. M. (2014). A 14-3-3 mode-1 binding motif initiates gap junction internalization during acute cardiac ischemia. *Traffic* **15**, 684-699.

Söhl, G. and Willecke, K. (2003). An update on connexin genes and their nomenclature in mouse and man. *Cell Commun. Adhes.* **10**, 173-180.

Solan, J. L. and Lampe, P. D. (2009). Connexin43 phosphorylation: structural changes and biological effects. *Biochem. J.* **419**, 261-272.

Sosinsky, G. E. and Nicholson, B. J. (2005). Structural organization of gap junction channels. *Biochim. Biophys. Acta* **1711**, 99-125.

Spagnol, G., Kieken, F., Kopanic, J. L., Li, H., Zach, S., Stauch, K. L., Grosely, R. and Sorgen, P. L. (2016). Structural Studies of the Nedd4 WW Domains and their Selectivity for the Connexin43 (Cx43) Carboxyl-terminus. *J. Biol. Chem.* **291**, 7637-7650.

Sun, P., Dong, L., MacDonald, A. I., Akbari, S., Edward, M., Hodgins, M. B., Johnstone, S. R. and Graham, S. V. (2015). HPV16 E6 controls the gap junction protein Cx43 in cervical tumour cells. *Viruses* **7**, 5243-5256.

Vanderpuye, O. A., Bell, C. L. and Murray, S. A. (2016). Redistribution of connexin 43 during mitosis. *Cell. Biol. Inter.* **40**, 387-396.

VanSlyke, J. K. and Musil, L. S. (2005). Cytosolic stress reduces degradation of connexin43 internalized from the cell surface and enhances gap junction formation and function. *Mol. Biol. Cell* **16**, 5247-5257.

Vaughan, D. K. and Lasater, E. M. (1990). Renewal of electrotonic synapses in teleost retinal horizontal cells. *J. Comp. Neurol.* **299**, 364-374.

Wang, X., Trotman, L. C., Koppie, T., Alimonti, A., Chen, Z., Gao, Z., Wang, J., Erdjument-Bromage, H., Tempst, P., Cordon-Cardo, C. et al. (2007). NEDD4-1 is a proto-oncogenic ubiquitin ligase for PTEN. *Cell* **128**, 129-139.

Ye, X., Wang, L., Shang, B., Wang, Z. and Wei, W. (2014). NEDD4: a promising target for cancer therapy. *Curr. Cancer Drug Targets* **14**, 549-556.

Zou, X., Levy-Cohen, G. and Blank, M. (2015). Molecular functions of NEDD4 E3 ubiquitin ligases in cancer. *Biochim. Biophys. Acta* **1856**, 91-106.

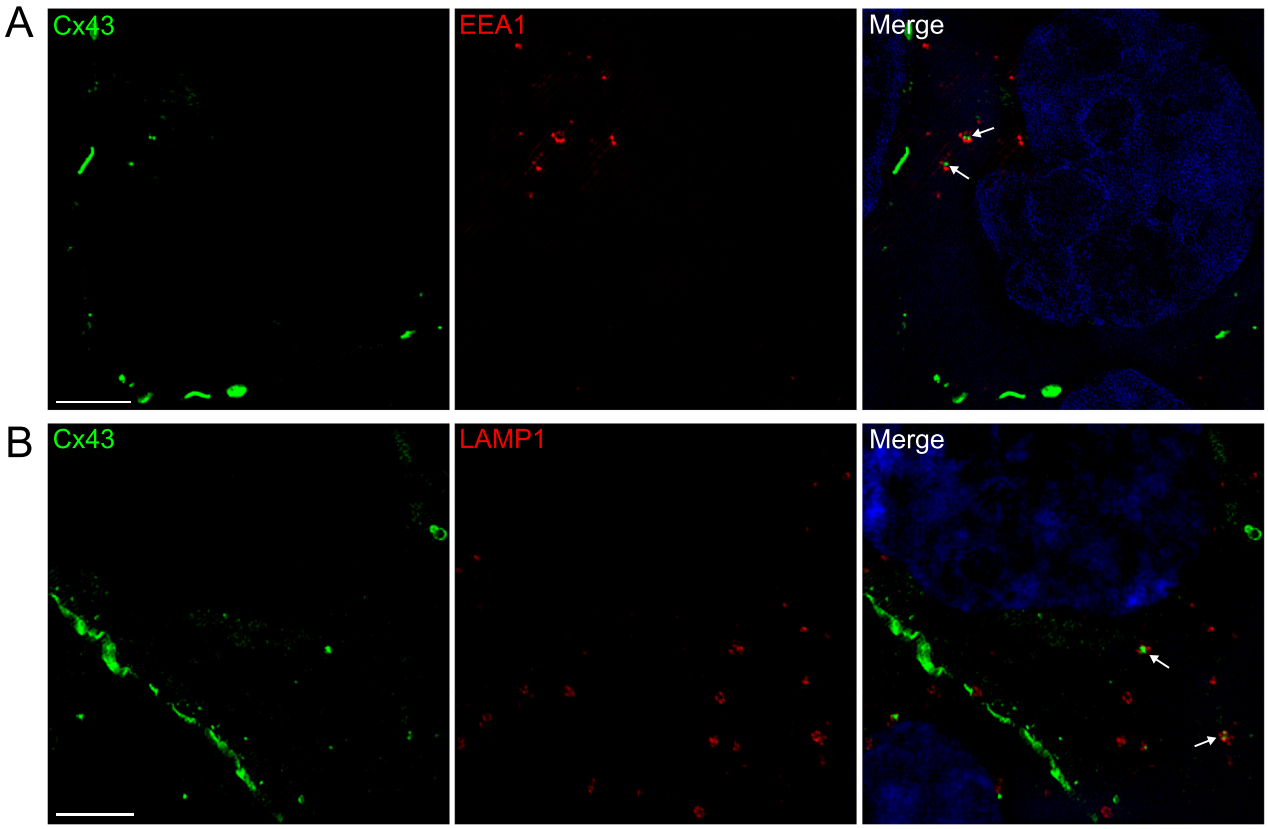

Supplementary Figure S1. Super-resolution microscopy analysis of the subcellular localization of Cx43 in HeLa-Cx43 cells. HeLa-Cx43 cells were fixed and stained with anti-Cx43 (green) in combination with either **(A)** anti-EEA1 (red) or **(B)** anti-LAMP1 (red) antibodies followed by Alexa488- and Alexa555-conjugated secondary antibodies. Nuclei were stained with Hoechst 33342 (blue). Cells were imaged by SIM. Arrows indicate localization of Cx43 in vesicular structures positive for EEA1 (A) or LAMP1 (B). Scale bar, 4 µm.

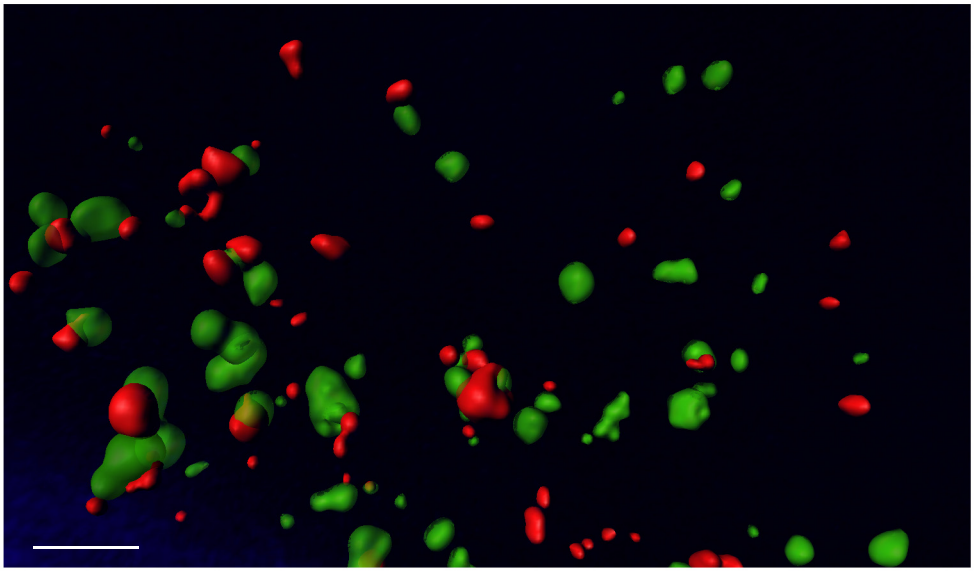

Supplementary Figure S2. Three-dimensional reconstruction of the subcellular localization of Cx43 and EEA1 in TPA-treated HeLa-Cx43 cells. HeLa-Cx43 cells were treated with TPA (100 ng/ml) for 90 minutes, fixed and stained with anti-Cx43 (green) and anti-EEA1 (red) antibodies followed by Alexa488- and Alexa555-conjugated secondary antibodies. Nuclei were stained with Hoechst 33342 (blue). Cells were imaged by SIM, and images were subjected to surface three-dimensional rendering using IMARIS. Scale bar, 1 µm.

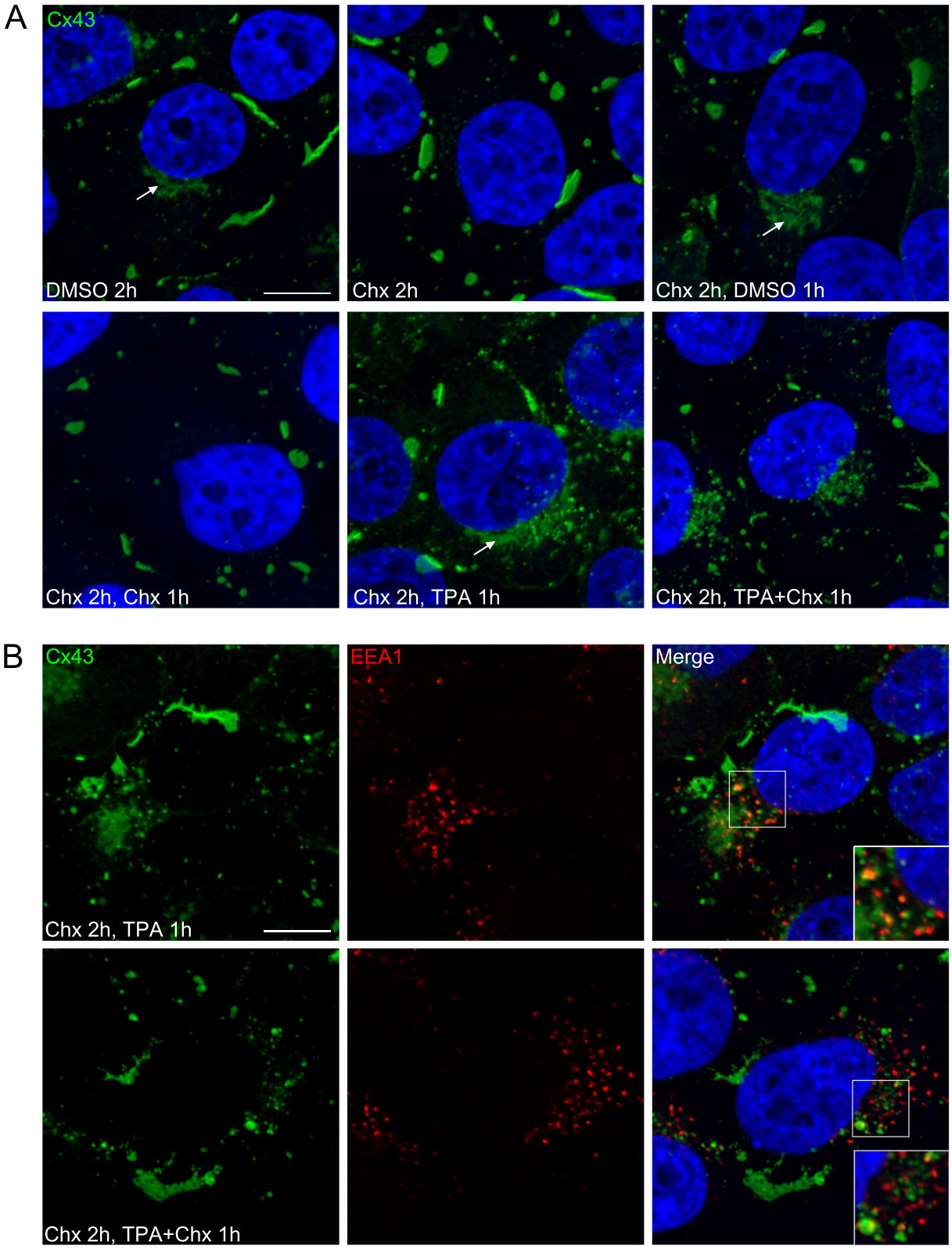

Supplementary Figure S3. Analysis of the subcellular localization of Cx43 in response to TPA treatment after preincubation with cycloheximide. (A) HeLa-Cx43 cells were treated with DMSO (solvent) or cycloheximide (Chx, 10 µM) for 2 hours, or preincubated with Chx (10 µM) for 2 hours followed by treatment with DMSO, Chx (10 µM), TPA (100 ng/ml) or Chx (10 µM) in combination with TPA (100 ng/ml) for 1 hour. Cx43 (green) was

analyzed by confocal microscopy. Arrows indicate diffuse perinuclear Cx43 staining, probably representing newly synthesized Cx43. Scale bar, 10 µm, applies to all images. **(B)** HeLa-Cx43 cells were preincubated with Chx (10 µM) for 2 hours followed by treatment with TPA (100 ng/ml) alone or with TPA (100 ng/ml) in combination with Chx for 1 hour. Cx43 (green) and EEA1 (red) were visualized by confocal microscopy. Scale bar, 10 µm, applies to all images.

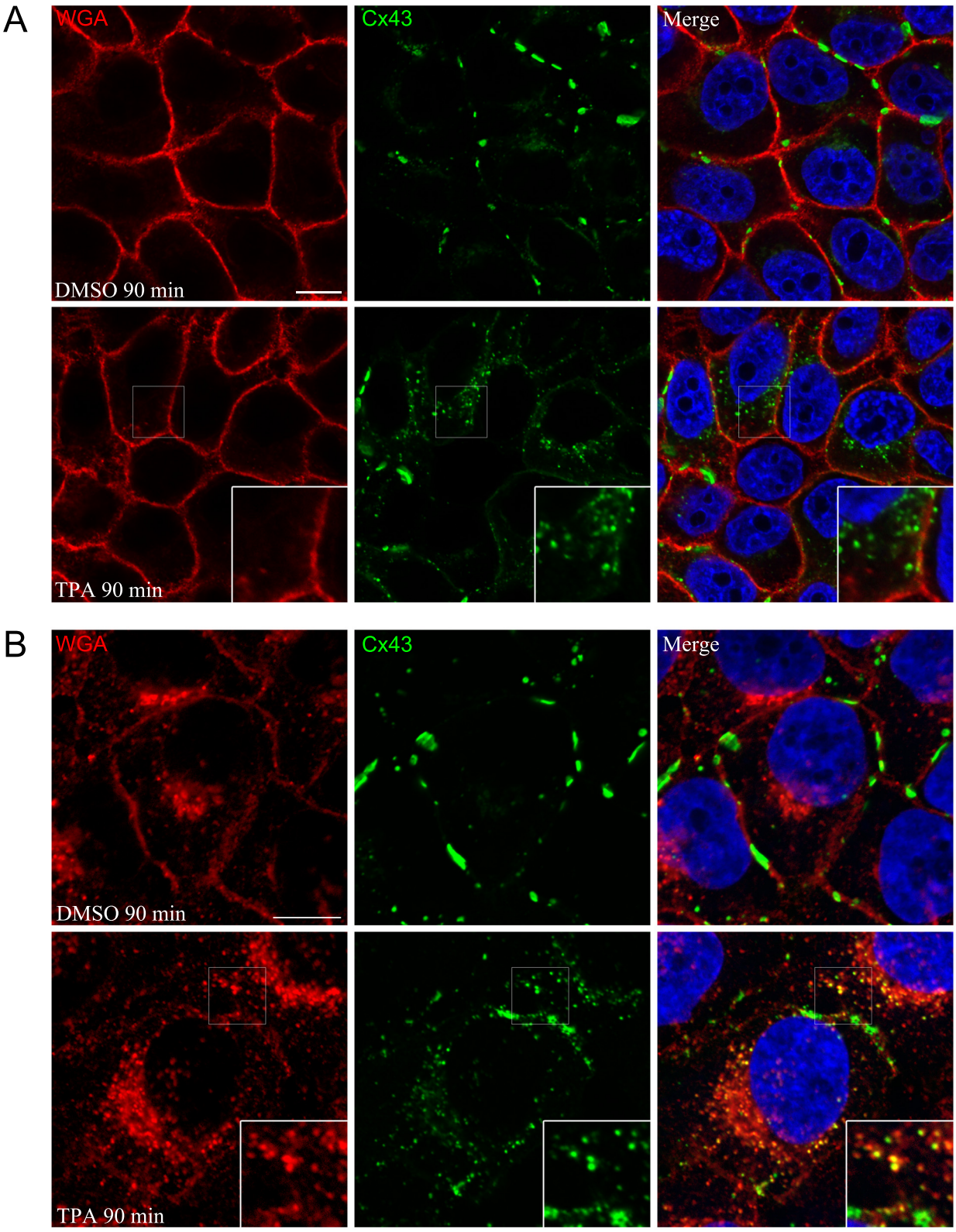

Supplementary Figure S4. Cx43 and WGA staining in HeLa-Cx43 cells. HeLa-Cx43 cells were **(A)** treated with either DMSO (solvent) or TPA (100 ng/ml) for 90 minutes and then incubated with Alexa555-conjugated WGA for 10 minutes to stain the plasma membrane or **(B)** incubated with Alexa555-conjugated WGA for 10 minutes to stain the plasma membrane and then treated with either DMSO (solvent) or TPA (100 ng/ml) for 90 minutes. Cx43 (green) and WGA (red) were visualized by confocal microscopy. Scale bars, 10 µm, apply to all images.

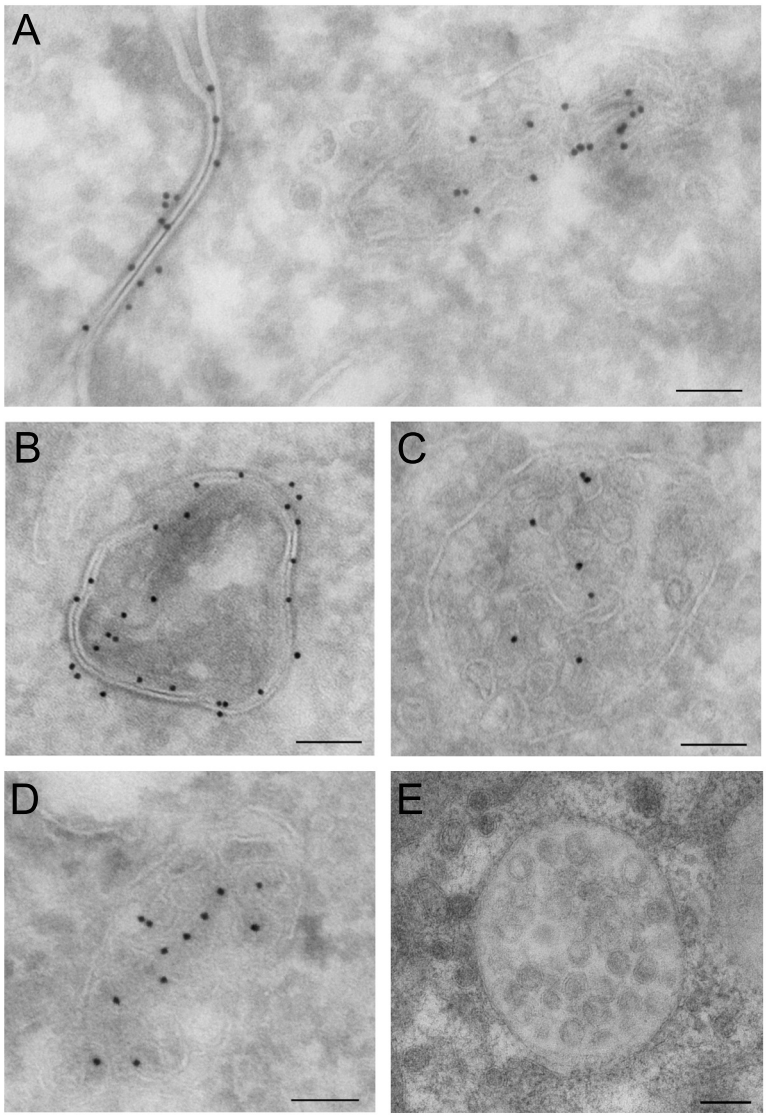

Supplementary Figure S5. Immunoelectron microscopy analysis of Cx43 localization in HeLa-Cx43 cells. Cells were left untreated **(A, D)** or treated with TPA (100 ng/ml) **(B, C)** for 60 minutes and fixed for immunoelectron microscopy. Ultrathin cryosections were labeled against Cx43 by using anti-Cx43 antibodies followed by incubation with 10 nm Protein A-gold particles. **(A)** Cx43 immunogold staining in a gap junction between two adjacent cells (left-hand side of the image) and in a multivesicular endosome (right-hand side of the image). **(B)** Cx43 immunogold staining in an annular gap junction. **(C, D)** Cx43 immunogold staining in multivesicular endosomes in TPA-treated **(C)** and untreated **(D)** HeLa-Cx43 cells. **(E)** For comparison, a multivesicular endosome as observed in cells that have been high-pressure frozen, freeze substituted, and embedded in Lowicryl, is shown. Scale bars, 100 nm.

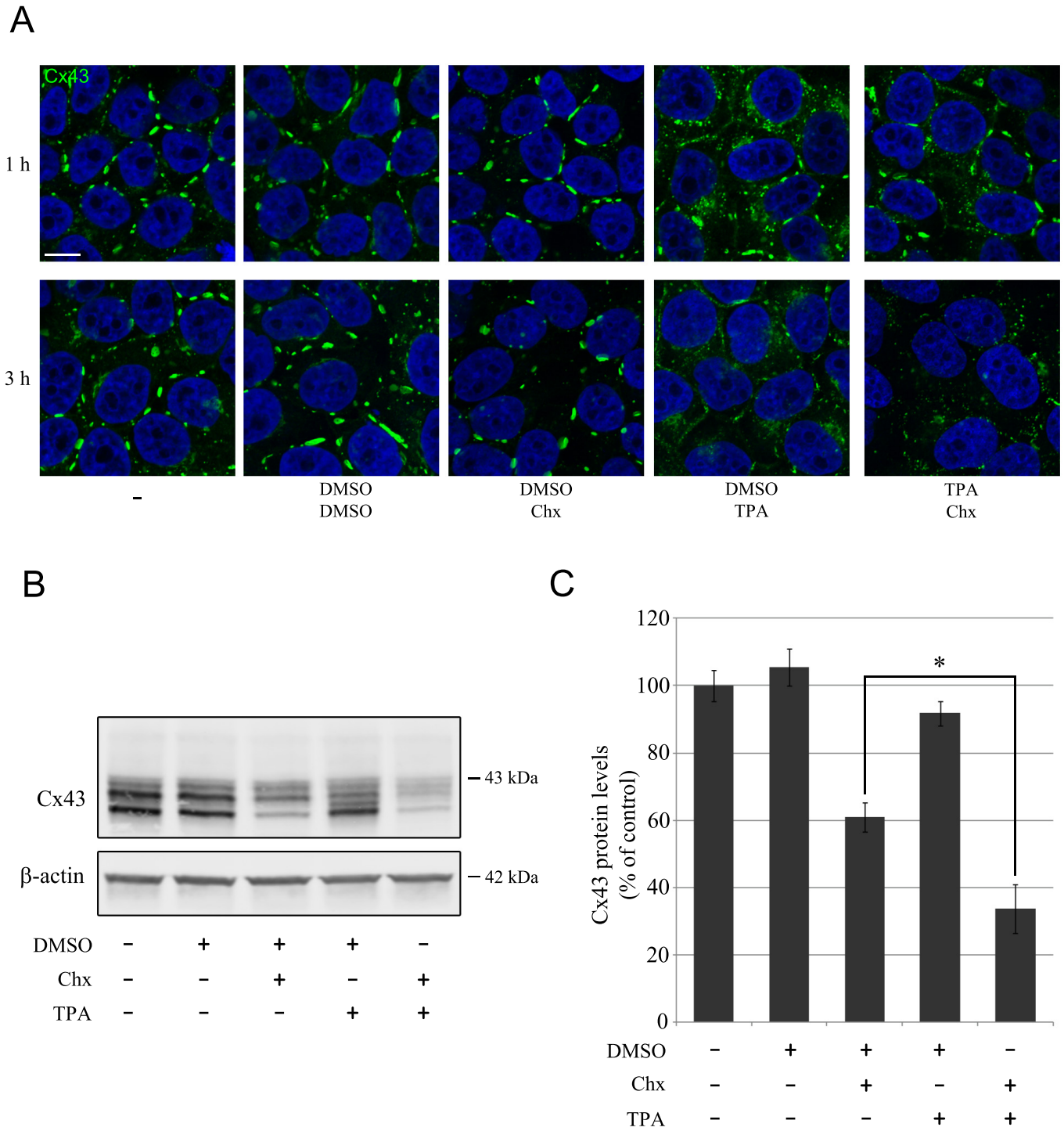

Supplementary Figure S6. Effect of TPA, Chx and DMSO gap junctions and Cx43 protein levels in HeLa-Cx43 cells. (A) HeLa-Cx43 cells were either left untreated, or treated with different combinations of TPA (100 ng/ml), Chx (10 µM) and DMSO (solvent) for 1 or 3 hours, as indicated. Cx43 (green) was then visualized by confocal fluorescence microscopy. Scale bar, 10 µm, applies to all images **(B)** HeLa-Cx43 cells were either left untreated, or treated with combinations of TPA (100 ng/ml), Chx (10 µM) and DMSO (solvent), in a similar manner as in A, for 3 hours. Cell lysates were then prepared, and equal amounts were subjected to SDS-PAGE. Cx43 and β-actin were detected by western blotting. Molecular mass in kDa is indicated. **(C)** The intensities of the Cx43 bands in B were quantified and normalized to the level of β-actin. Values shown are the means ± S.E.M. of three independent experiments. *$p<0.05$

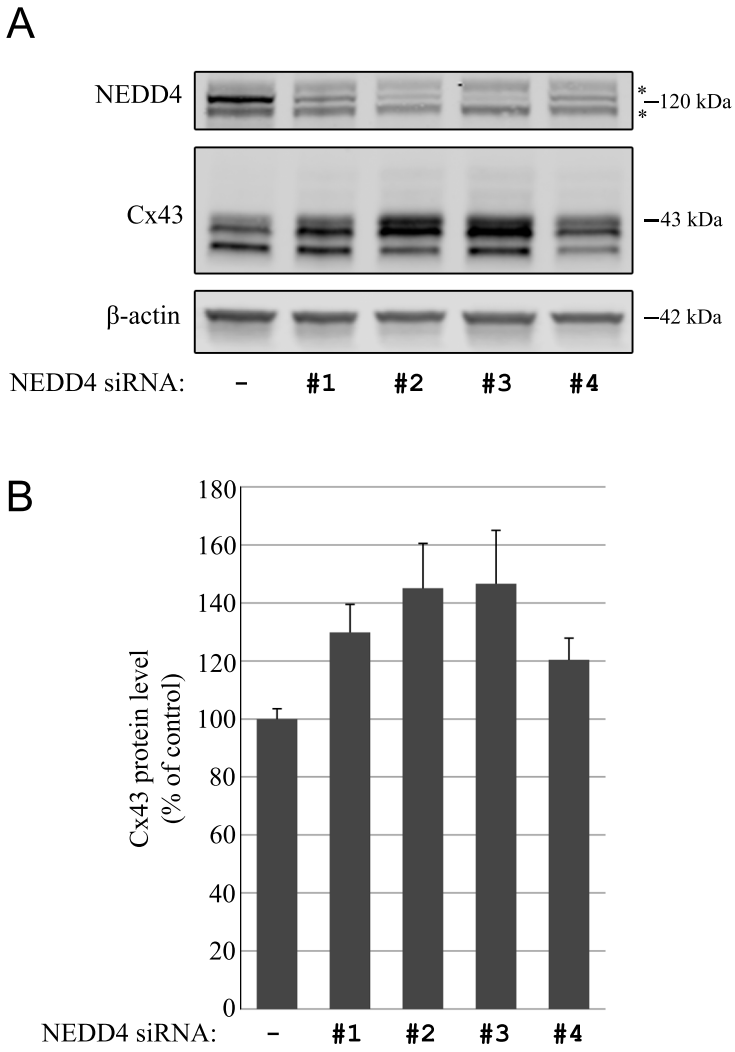

Supplementary Figure S7. Effect of siRNA-mediated depletion of NEDD4 on Cx43 protein levels. HeLa-Cx43 cells were transfected with control siRNA or with four different siRNA sequences against NEDD4. Cell lysates were prepared 96 hours after transfection, and equal amounts of total cell protein lysates were subjected to SDS-PAGE. NEDD4 and Cx43 were detected by western blotting using antibodies against NEDD4 and Cx43, respectively **(A)**. The membranes were also probed with antibodies against β-actin as a gel-loading control. The intensities of the Cx43 bands on western blots were quantified and normalized to the β-actin level **(B)**. Asterisks indicate unspecific bands. Values shown are the mean ± S.E.M of three independent experiments. Molecular mass in kDa is indicated.

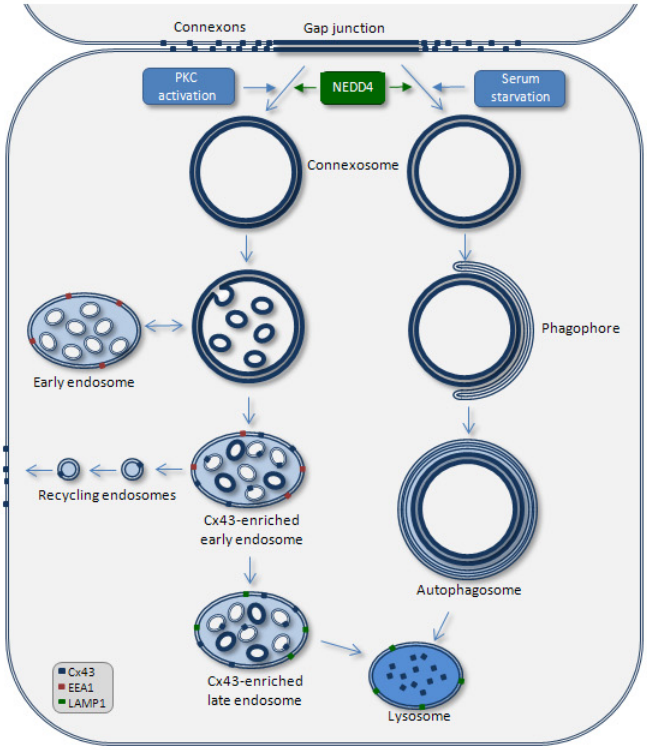

Supplementary Figure S8. Model of the role of NEDD4 in sorting of Cx43 from the plasma membrane to lysosomes. On the basis of the present and previous studies from our laboratory and other laboratories, we propose a model in which Cx43 is able to follow two distinct pathways en route to lysosomes following gap junction internalization. In the first pathway, connexosomes (i.e. annular gap junctions) undergo fusion with early endosomes. This fusion process is associated with the transformation of the connexosome from a double-membrane vacuole to a Cx43-enriched multivesicular endosome, which will eventually fuse with a lysosome. In the second pathway, connexosomes are enclosed by a phagophore, resulting in the formation of an autophagosome, which subsequently fuses with a lysosome. In this model, both pathways are involved in the degradation of Cx43 under basal conditions, and their relative importance is likely to differ between different cell types. Furthermore, the degradation of Cx43 along each of these pathways may be affected differently in response to changes in the intracellular or extracellular environments. For instance, activation of PKC promotes endocytosis and degradation of Cx43 along the endolysosomal pathway. On the other hand, serum starvation induces endocytosis and degradation of Cx43 along the autophagosomal pathway. Both the PKC- and serum-starvation-induced degradation of Cx43 are associated with increased Cx43 ubiquitination. Furthermore, NEDD4 is involved in both the PKC-induced degradation of Cx43 along the endolysosomal pathway and the serum-starvation induced degradation of Cx43 along the autophagosomal pathway.